EFFECT OF PELLET-CLADDING INTERACTION (PCI) AND DEGRADATION

MECHANISMS ON SPENT NUCLEAR FUEL ROD MECHANICAL

PERFORMANCE DURING TRANSPORTATION

by

Rishav Poudyal

A thesis submitted to the faculty of
The University of Utah
in partial fulfillment of the requirements for the degree of

Master of Science

Department of Civil and Environmental Engineering

The University of Utah

August 2016

The University of Utah Graduate School

STATEMENT OF THESIS APPROVAL

The thesis of **Rishav Poudyal**

has been approved by the following supervisory committee members:

Luis F. Ibarra	, Chair	**04/29/2016**	Date Approved
Chris P. Pantelides	, Member	**04/29/2016**	Date Approved
Amanda Bordelon	, Member	**04/29/2016**	Date Approved

and by **Michael E. Barber** , Chair of

the Department of **Civil and Environmental Engineering**

and by David B. Kieda, Dean of The Graduate School.

ABSTRACT

This study evaluates the structural integrity of spent nuclear fuel (SNF) rods under impacts caused by accidents during transportation. SNF rods consist of uranium dioxide fuel pellets encapsulated in a zircaloy cladding tube. The linear and nonlinear buckling analysis of a typical 532 mm (21 in.) long fuel rod segment is performed in finite element software Abaqus, under static loading conditions. Initially, the analysis is carried out for a vertical end drop, including an initial imperfection of 0.1 mm in the model. Thereafter, impact drops are evaluated with the fuel rod at different orientations. The results indicate that pellets significantly stiffen the fuel rod when its orientation is nearly vertical. However, the pellet contribution decreases significantly as the orientation angle at impact increases. The effect of pellet-cladding interaction (PCI) on the buckling performance of the SNF rods is also studied. The results indicate that the PCI composite action is partially retained even for relatively large rod impact angles with respect to the vertical direction.

The inelastic buckling controls the buckling behavior of the fuel rods with lower slenderness ratio. Therefore, the effect of degradation mechanisms of the irradiated clad after long-term storage are considered on the buckling behavior of 252 mm (10 in.) and 140 mm (5.5 in.) fuel rod segments. The study concludes that long-term degradation only affects the 140 mm simply supported fuel rod segment, length equivalent to the end cantilever segment. However, this segment is not expected to fail because its buckling capacity is one order of magnitude higher than that of a typical 532 mm segment.

TABLE OF CONTENTS

LIST OF TABLES

LIST OF FIGURES

ACKNOWLEDGEMENTS

I am particularly indebted to my advisor, Dr. Luis Ibarra, for his relentless support and guidance during my research, preparation of my thesis, and throughout the graduate program. It is an absolute pleasure learning and working with him.

I would like to express my sincere gratitude to the supervisory committee members, Dr. Chris Pantelides and Dr. Amanda Bordelon, for being part of my graduate committee and providing assistance throughout the MS program.

I am very thankful to Uma Ramasamy for helping me with Abaqus, literature review, and research as a whole.

Finally, my appreciation would be incomplete without expressing gratitude towards my family, for all the love and support.

CHAPTER 1

INTRODUCTION

1.1 General Overview – Spent Nuclear Fuel (SNF)

A nuclear power plant (NPP) produces a large amount of energy from the nuclear fission reaction inside the nuclear reactor. The energy produced is used to heat and convert water into steam that drives the turbine, thus producing electricity. Pressurized Water Reactors (PWRs) and Boiling Water Reactors (BWRs) are the most common reactors.

A nuclear reactor includes fuel assemblies with fuel rods arranged in a square array, laterally supported with spacer grids. The fuel rods consist of fuel pellets enclosed in a Zircaloy cladding tube. There are guide tubes within the arrangement of the fuel rods to control the amount of fission reaction. After the production of energy from the nuclear fission reaction, the spent nuclear fuel (SNF) rods are initially stored in pools adjacent to the reactor to lower their temperature, and prevent melting of the Zircaloy cladding.

1.2 Interim Spent Fuel Storage Installations (ISFSIs)

When the temperature of the fuel assemblies decreases, the SNF rods are transferred from pool to dry storage casks at sites contiguous to nuclear power plants, known as interim spent fuel storage installations (ISFSIs). ISFSIs were initially licensed for compliance periods of 20 years, but recently, it has been considered to increase the licensing period

up to hundreds of years. Therefore, the effect of degradation mechanism resulting from the long-term storage has to be considered.

1.3 Literature Review

1.3.1 Fuel Rod Failure Modes

There could be several potential fuel rod failure modes during accidents. For instance, Sanders et al. (1992) considered three potential fuel rod failure modes. Failure mode A is a transverse crack in the cladding, which can occur due to large strains beyond the clad ductility limits. Failure mode B is an extension of failure mode A that occurs if the strain energy is large, causing rod breakage. Failure mode C is a longitudinal tearing of the cladding. The crack is initiated at the inner surface of the cladding due to pellet-cladding interaction (PCI) cracking or manufacturing flaws. Failure C refers to large localized pinch forces develop at the location of spacer grids in the fuel rod during side drops. Hydride reorientation affects the failure mode C as it reduces the clad ductility when pinching loads are developed.

1.3.2 Buckling Failure

Potential accidents during cask transportation can lead to impact loads on SNF rods resulting in buckling failure. Buckling is characterized by a sudden sideways failure of a structural member subjected to high compressive stress.

Euler's buckling formulation can be used to find the fuel rod critical buckling load.

The theoretical critical buckling load P_{cr} is given as:

$$P_{cr} = \frac{\pi^2 EI}{(KL)^2} \qquad (1)$$

where,

E= modulus of elasticity

I =moment of inertia about the buckling axis

K =the effective length factor based on end boundary conditions

L= unsupported length of the member

To account for the geometric nonlinearities, however, nonlinear buckling analysis is required for which Riks analysis is performed in Abaqus to find the rod critical load and the postbuckling response. Nonlinear buckling analysis using Riks method provides a more accurate prediction of fuel rods that exhibit gaps between pellets and cladding.

1.4 Objectives

The study evaluates the structural integrity of spent nuclear fuel (SNF) rods in an impact accident scenario during transportation after long-term storage. The SNF rod evaluation includes the effect of PCI and degradation mechanism on the buckling behavior of SNF rods. Nonlinear buckling analysis using Riks method is used in Abaqus to access the buckling behavior of SNF rods.

CHAPTER 2

QUASI-STATIC BUCKLING – EFFECT OF PCI

2.1 FE Model Description and Inputs

A fuel assembly contains several fuel rods arranged in a square array, laterally supported at the grid spacer's location. Depending on the fuel assembly configuration, these supports are usually located every 381 - 635 mm (15 - 25 in.), except at the end cantilever segment of the rods, which may have end cantilever lengths of 51 - 76 mm (2 - 4 in.) (DOE, 1987). The initial fuel rod configuration consists of uranium pellets (UO_2) inserted into a cladding tube (Zr-4) with a small radial gap of 80 µm between them. This gap tends to close once the fuel rod is irradiated and subjected to high temperatures in the reactor. The fuel rod performance is expected to be significantly affected by pellet-cladding interaction (PCI).

This section evaluates the buckling behavior of a 532 mm (21 in.) fuel rod segment considering linear and nonlinear material properties, where 532 mm is the length corresponding to the most common length between grid spacers in a Westinghouse W17 × 17 fuel assembly. The models also incorporate the effect of PCI on the buckling capacity of fuel rods. The pellet and clad dimensions were obtained from the INL/CON-09-15677 report (Williamson and Knoll, 2009), and are presented in Table 2.1.

2.1.1 Finite Element (FE) Mesh

The mesh shown in Fig. 2.1 was generated with C3D8R elements (solid reduced integration linear brick elements) for fuel pellets and C3D8I (solid linear continuum shell elements) for the cladding. The C3D8I elements are appropriate to characterize bending behavior, even when only one element is utilized through the thickness (Brown, 1997). The C3D8R element with relatively coarser mesh can be chosen for a complex structure involving interactions (Zhan and Li, 2013).

2.1.2 Material Properties

The fuel rod consists of zircaloy-4, Zr-4 cladding (US DOE, 1987), which contains uranium dioxide, UO_2 pellets. The material properties used in the FE model for UO_2 (Table 2.2) are based on the FCRD-UFD-2013-000325 report (Adkins et al., 2013). Engineering stress-strain data (Matweb, 2015) was used to calculate true stress - plastic strain data, which was used as input in the FE model. Equations (2), (3), and (4) were used to find the required inputs. Fig. 2.2 shows engineering and true stress-strain curves.

$$\sigma_{tru} = \sigma_{nom}\left(1 + \epsilon_{nom}\right) \tag{2}$$

$$\epsilon_{tru} = ln\left(1 + \epsilon_{nom}\right) \tag{3}$$

$$\epsilon_{pl} = \left(\epsilon_{tru} - \frac{\sigma_{tru}}{E}\right) \tag{4}$$

2.1.3 Boundary Conditions and Interactions

The fuel rod is pin-connected at its base, allowing free rotation, but prevents translation. At the top, it is free to translate in the direction of the longitudinal axis of the

fuel rod (Z axis), in addition to free rotation. The pin connection is a model simplification for the spacer grids, which allow certain lateral displacement between fuel rod and spacer boundary.

Reference points (RPs) are defined and coupled to the desired surfaces via coupling constraints (Fig. 2.3). Reference point RP1 is coupled to the clad bottom surface, allowing free rotation, but preventing translation. At the top surface, reference points RP2 and RP3 are coupled to the cladding and pellet top surfaces, respectively. The bottom end of the fuel rod is closed, whereas the top end is open. RP2 and RP3 allow free rotation, but are restrained to translate in the X and Y directions, only allowing translation in the direction of the longitudinal axis of the fuel rod (Z direction).

2.2 Buckling Analysis of 532 mm (21 in.) Fuel Rod

The numerical simulations are carried out in Abaqus, both for linear eigenvalue and nonlinear buckling analysis. The effect of PCI is also incorporated in the model. Three different cases are studied.

1) Pellet-cladding radial gap of 80 μm and pellet-pellet in contact (Case 1)

2) Pellet-cladding interaction (PCI) and pellet-pellet in contact (Case 2)

3) PCI and pellet-pellet bonded (Case 3)

2.2.1 Linear Eigenvalue Buckling Analysis

Eigenvalue buckling analysis of the fuel rod is performed using a linear perturbation technique in Abaqus, controlled by STATIC, GENERAL command. The linear buckling model can be used to include the imperfection in the nonlinear model from

the superposition of eigen mode of the linear model. The linear perturbation technique is compared with a benchmark analytical solution for a single pellet fuel rod of 532 mm with pinned boundary conditions at both ends.

The theoretical Euler buckling load for the 532 mm fuel rod, assuming pinned end conditions with K = 1, is calculated as 2,887 N. This is only 0.9% higher than the value 2,862 N (Table 2.3) obtained from the linear eigenvalue analysis of Case 3. The moment of inertia (I) is calculated considering PCI and pellet-pellet bonded condition, assuming the clad and pellets are concentric. The buckling capacities of the 532 mm fuel rod from eigenvalue analysis for different cases are presented in Table 2.3 and the buckling mode is shown in Fig. 2.4. Case 3 is highly unlikely to occur because of the very low tensile strength of 100 MPa of pellets versus 690 MPa of clad and initially cracked state of pellets (Sanders et al., 1992).

Table 2.3 also shows the buckling capacity in terms of "g", which was computed based on the fuel rod mass. Note that an impact deceleration of 118 g. is required to exceed the Euler buckling capacity of 2,887 N, considering that SNF rod WE 17 × 17 self-weight is 24.43 N/fuel rod. Ramsey et al. (1987) reported a deceleration of 82 g. at initial storage for end drop tests of storage casks. They recommended a deceleration limit of 82 g. for SNF rods at initial storage, and 95 g. after 20 years of storage, as modulus of elasticity increases when temperature reduces at later age.

2.2.2 Riks Nonlinear Buckling Analysis

Nonlinear buckling analysis of the fuel rod was performed using the STATIC, RIKS method in Abaqus, a method based on the arc length approach. Nonlinear buckling

analysis using Riks method provides a more accurate prediction of fuel rods that have a gap between cladding and pellets, or not full composite action between the components. Riks method can also be used to study the rod's postbuckling response.

Geometric imperfections are introduced in the nonlinear model by linear superposition of Eigen buckling modes from the linear model. A geometric imperfection is introduced as a parabolic deflection profile with a deflection of 0.1 mm at the middle of the fuel rod. Load-displacement curves of nonlinear buckling analysis with an initial imperfection of 0.1 mm for Cases 1, 2, and 3 are shown in Fig. 2.5. The force is measured at RP3 in the Z direction while the displacement is measured at the center of the middle pellet in the X direction. Table 2.4 presents the summary of the buckling capacities of the 532 mm fuel rod with 0.1 mm imperfection and the maximum Von Mises (VM) stresses.

As observed in Fig. 2.5, the presence of pellets in Case 1, even without PCI effects, increases the buckling capacity almost three times with respect to that of the clad only segment. However, after the bifurcation point the strength of the Case 1 rod rapidly decreases and approaches the buckling capacity of the clad only segment. Therefore, the additional Case 1 buckling capacity provided by the pellets can only be considered if the segment is constrained in the midsection, and the fuel rod can only move 2 or 3 mm. If the pellets are bonded to the cladding, as in the Case 2 segment, the rod buckling capacity increases 20%, from 2,173 N to 2,624 N. The strength reduction of Case 2 after the bifurcation point is less pronounced (only about 20%) than that of Case 1. This is the main benefit of the PCI composite action. The capacity of Case 3 only increases 5% compared to that of Case 2. The main effect of pellet-pellet bonding is on the rod's stable postbuckling behavior.

Table 2.4 also shows that the stresses for all the cases are about 20% the material's yield strength of 381 MPa. This result proves that the buckling behavior of the 532 mm fuel rod is controlled by elastic buckling because of its large slenderness ratio (KL/r =143). It can also be corroborated by the fact that the load-displacement plot with the linear and nonlinear material properties overlapped. Therefore, the 532 mm fuel rod would fail because of elastic instability before yield strength is achieved.

2.3 Probability Distribution of Cask Impact Angles

The hypothetical accident scenario presented in Section 2.2 assumes that the cask impacts vertically onto the ground. However, casks are usually transported with the longitudinal axis in a horizontal condition. Therefore, most impacts during accident scenarios are likely to have a small angle of impact between the longitudinal axis and the surface. Fig. 2.6 shows a step-wise probability distribution of impact angles to the horizontal proposed by John (2014) in the NUREG report. As observed, the probability of the drop with impact angles around 80-90° (i.e., relatively vertical impacts) is very low at around 0.02. However, there is a high probability of about 0.2 for impact angles between 0-10° (i.e., relatively horizontal impacts). Therefore, the buckling behavior assessment at different fuel rod inclinations is required.

2.4 Buckling Capacity for Different Fuel Rod Inclinations

The fuel rod buckling capacity and postbuckling behavior may be affected by normal loading caused by rod inclination with respect to the vertical direction at the time of impact. This section evaluates the capacity of a 532 mm segment with various

inclinations with respect to the vertical direction. A rod inclination during impact will add a rod normal component force due to its self-weight. This normal component will create a deflection profile in addition to the expected initial imperfections, reducing the fuel rod buckling capacity.

For rods with an inclination at impact time, the segment's self-weight was also incorporated in the vertical direction. For instance, the evaluated segment is assumed to be the bottom segment of a seven 532 mm segment-fuel rod. In the vertical direction, $6/7^{th}$ of the load was applied as a concentrated load at the top of the fuel rod segment, representing the above six segments, whereas $1/7^{th}$ of the load was applied as a self-weight at the bottom segment. Fig. 2.7 shows the rod inclined at 15° with respect to the vertical.

The self-weight normal component was applied as a series of concentrated loads normal to the longitudinal axis. The concentrated load on the top was distributed proportionately to the pellet and clad according to their self-weight, i.e., 85% was applied to the pellet via RP3 and 15% to the clad via RP2.

2.4.1 Application of the Normal Loading

The normal loading is applied in the direction perpendicular to the rod longitudinal axis, i.e., in the X direction. The force is measured in Z direction at RP3, while the displacement is measured at the center of the middle pellet in the direction of application of the lateral load, or X direction. Because the self-weight is evenly distributed along the rod's length, the normal load was distributed in 37 different loading points at every 14 mm, coinciding with the pellet length (Fig. 2.8).

Figs. 2.9 and 2.10 present the vertical force-lateral displacement curves for Cases

1 and 2, respectively, under different inclinations during impact. The results show that the beneficial effect of fuel pellets in terms of buckling capacity is significantly reduced as the rod inclination increases. For Case 1, the buckling capacity under only vertical loading is 2,170 N, but it is reduced to 1,140 N for a 15° inclination, a reduction of almost 50%. As expected, as inclination angles increase, the fuel rod buckling capacity decreases. It will be shown that this decrease is accelerated by a lower contribution of the pellets.

The contribution of pellets in the buckling capacity of the fuel rod at different inclination angles can be better understood by computing the buckling capacities of the clad. Fig. 2.11 presents the force-displacement curves for cladding only, which also indicates a reduction in capacity as the impact angle increases. The force-displacement comparison of Cases 1 and 2 to cladding is shown in Figs. 2.12 and 2.13. However, the effect of pellets for different inclination angles is better understood when the data are normalized.

2.5 Normalization of Case 1 and 2 Fuel Rods

The normalization of buckling capacity of Case 1 and 2 fuel rods with respect to that of clad only is presented in Table 2.5. The results show that the fuel rod capacity decreases faster than that of clad only, as the orientation angle increases.

Figs. 2.14 and 2.15 present the normalized Case 1-to-clad and Case 2-to-clad force-displacement curves, respectively. Fig. 2.16 shows both normalizations. For small displacements, Case 1-to-clad only ratios exhibit larger ratios that rapidly decrease and stabilize at about 1.5 for all the orientation angles. The stabilization at a ratio of about 1.5 for Case 1, for horizontal (or quasi-horizontal) impact conditions, is mainly caused by the

pellets being in perfect contact in the FEM. The large initial values indicate that pellets greatly stiffen the fuel rod when the orientation is almost vertical (zero degree angle). However, as the orientation angle at impact increases, the pellet contribution decreases. Case 2-to-clad only ratios approach a value of about 2.5 for large displacements, indicating that PCI composite action is partially retained even for relatively large orientation angle.

Table 2.1: Dimensions of fuel rod

Dimension	Value (mm)
Length of clad	532.00
Outer diameter of clad	10.54
Clad thickness	0.60
Clad inner diameter	9.34
Length of pellet	14.00
Pellet diameter	9.18

Table 2.2: Material properties of fuel rod (Adkins et al., 2013)

Properties	Zr-4	Uranium Dioxide
Young's Modulus, E (N/mm^2)	99,300	166,000
Poisson's ratio, μ	0.37	0.21
Density $(tonne/mm^3)$	6.59E-09	1.03E-08

Table 2.3: Buckling capacity of 532 mm fuel rod from Eigen value analysis

Configuration	Buckling capacity (N)	Buckling capacity (g)
Clad only	771	32
Case 1	2546	104
Case 2	2774	114
Case 3	2862	117

Table 2.4: Buckling capacity of 532 mm fuel rod from nonlinear analysis

Configuration	Buckling capacity (N)	Max VM Stresses (MPa)
Case 1	2173	69.35
Case 2	2624	76.64
Case 3	2769	80.11

Table 2.5: Summary of the buckling capacities of 532 mm fuel rod

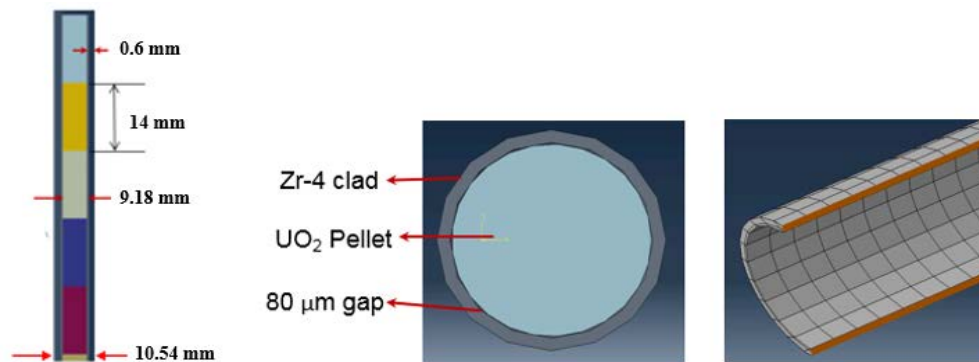| Inclination to the vertical	Buckling capacity (N) Clad only	Buckling capacity (N) Case 1	Normalized capacity of Case 1 with respect to clad	Buckling capacity (N) Case 2	Normalized capacity of Case 2 with respect to clad
0	771	2173	2.80	2624	3.40
3	755	1750	2.32	1907	2.53
15	646	1140	1.76	1594	2.47
30	628	980	1.56	1345	2.14
45	567	846	1.49	1132	2.00
60	485	699	1.44	902	1.86
75	349	483	1.38	600	1.72

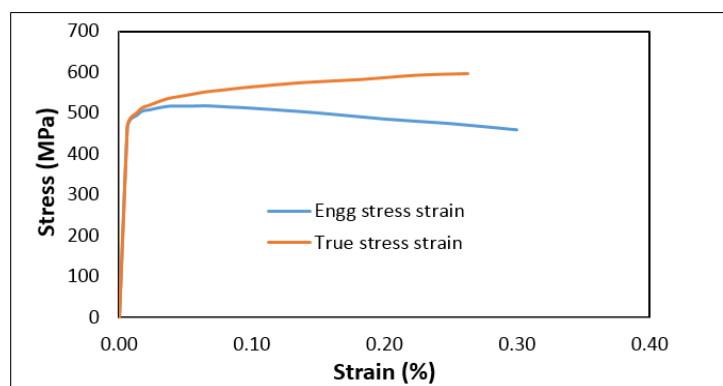Fig. 2.1: Dimensions of fuel rod (a) elevation (b) cross section

Fig. 2.2: Stress-strain curves of unirradiated Zr-4 cladding
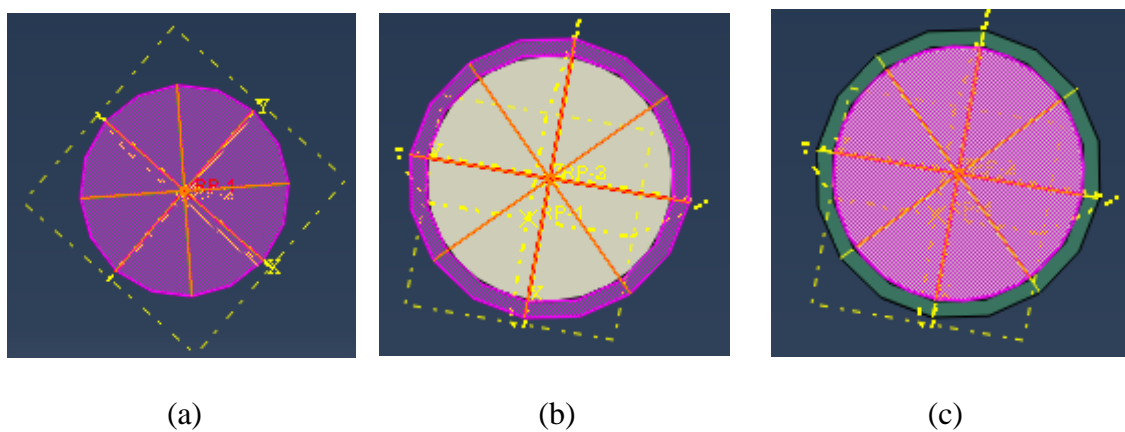

| (a) | (b) | (c) |

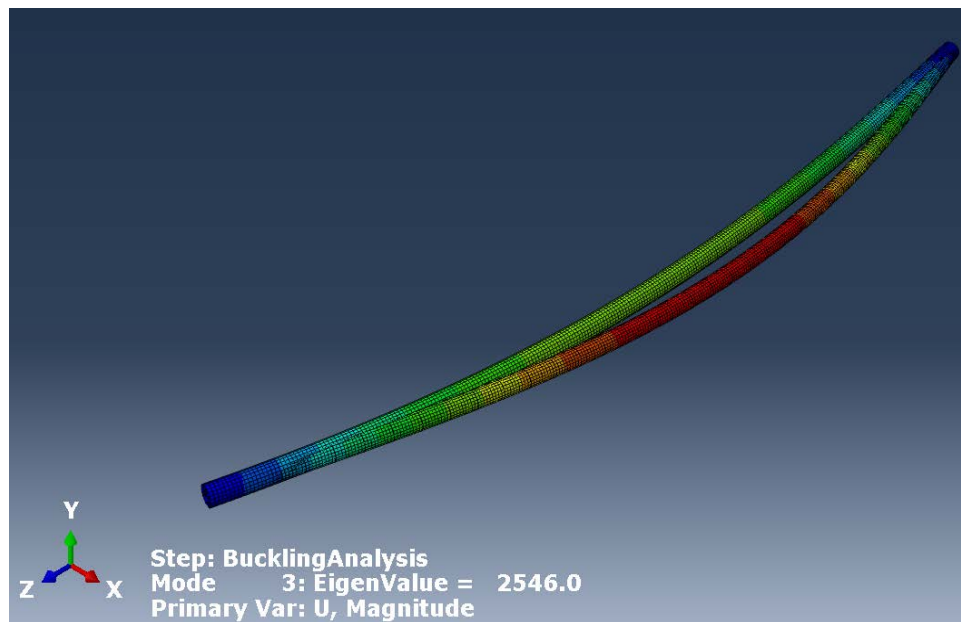Fig. 2.3: Coupling constraints. (a) RP1, (b) RP2, (c) RP3

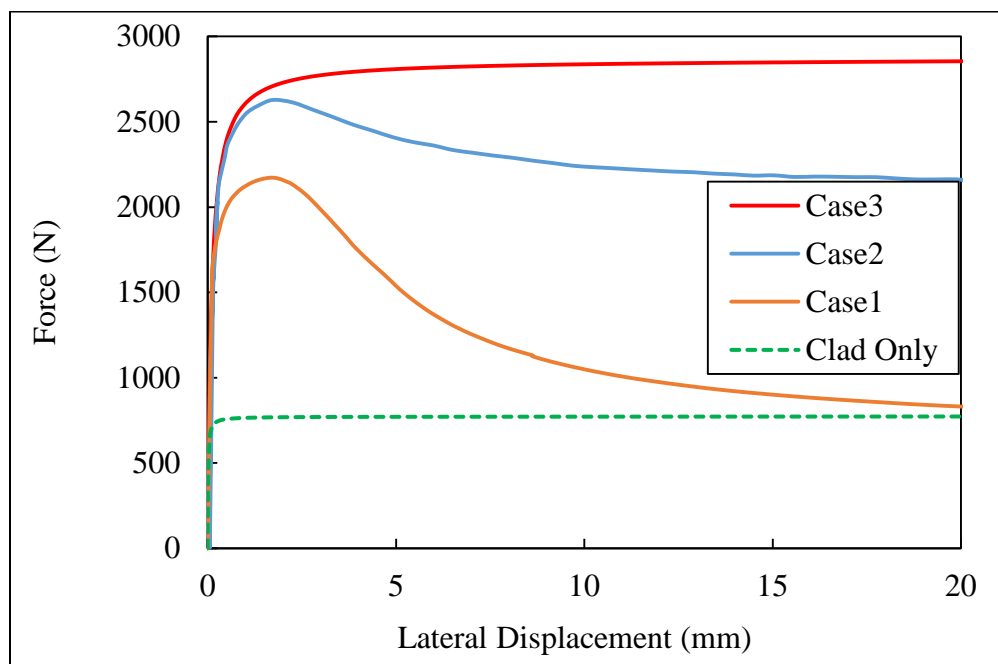Fig. 2.4: Buckling mode for Case 1 vertical case

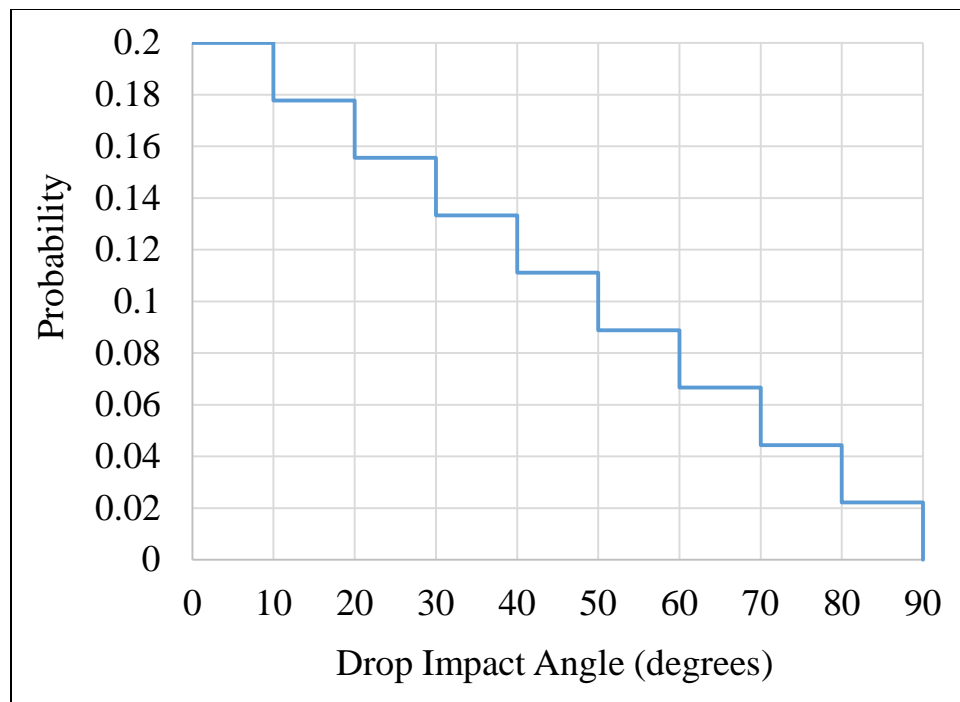Figure 2.5: Load-displacement plots at center of mid pellet for 0.1 mm imperfection

Fig. 2.6 Probability distribution of impact angles to the horizontal (after NUREG, 2014)
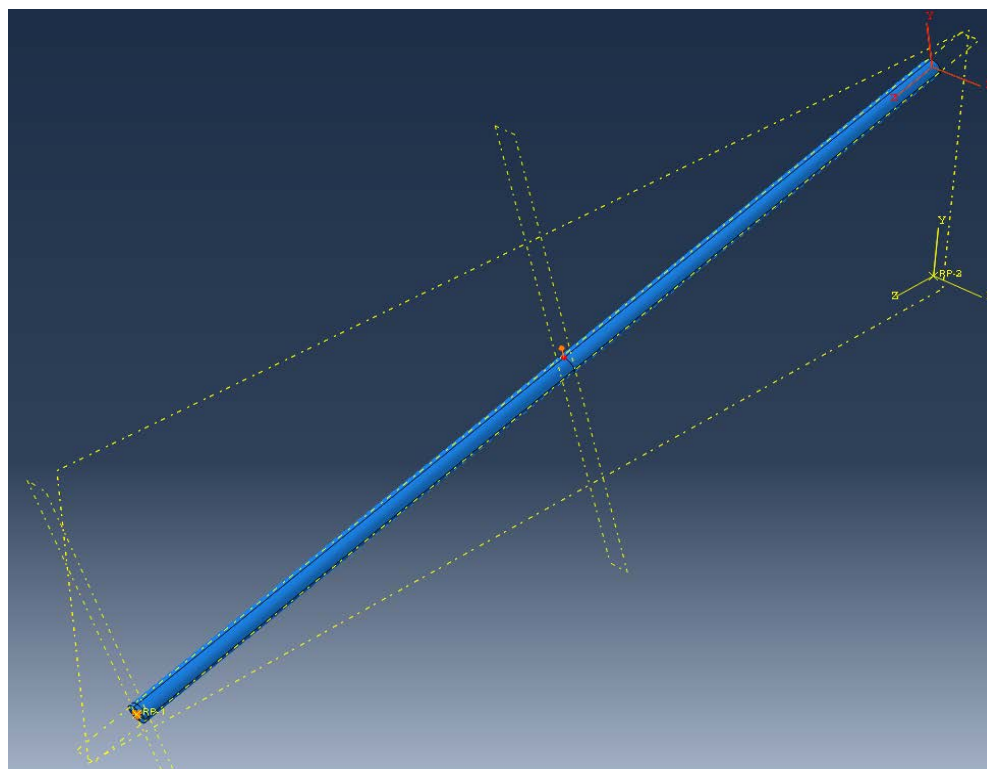

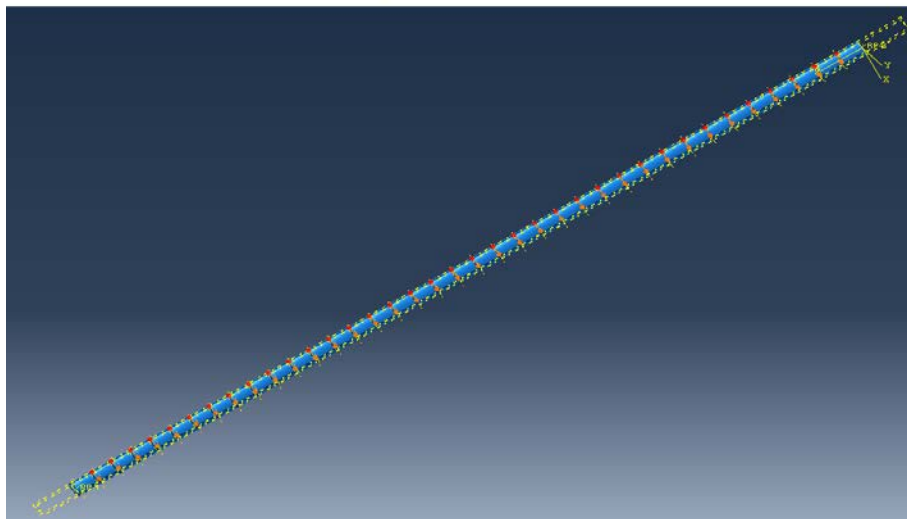Fig. 2.7: Fuel rod of 532 mm length inclined 15° from longitudinal axis at impact

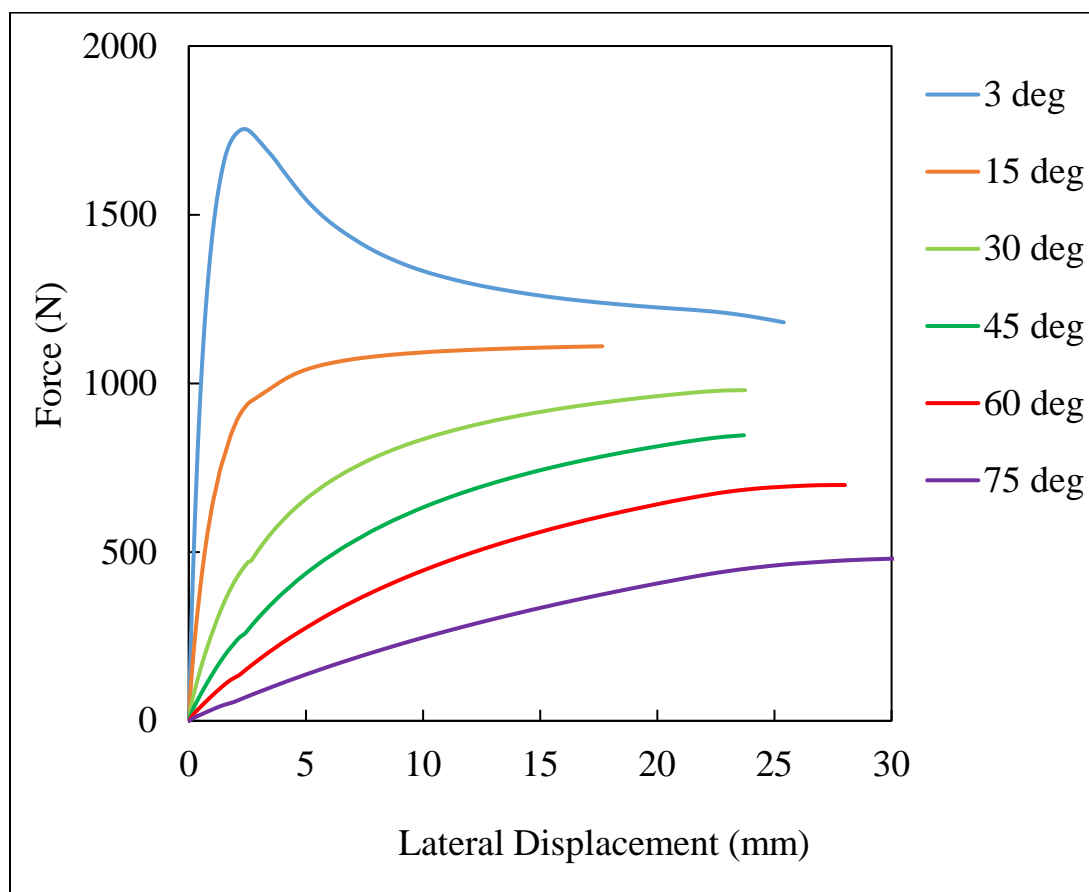Fig. 2.8: Application of point loads in 37 loading points simulating a distributed load

Fig. 2.9: Force-displacement plots of 532 mm fuel rod for Case 1 with inclinations

Fig. 2.10: Force-displacement plots of 532 mm fuel rod for Case 2 with inclinations

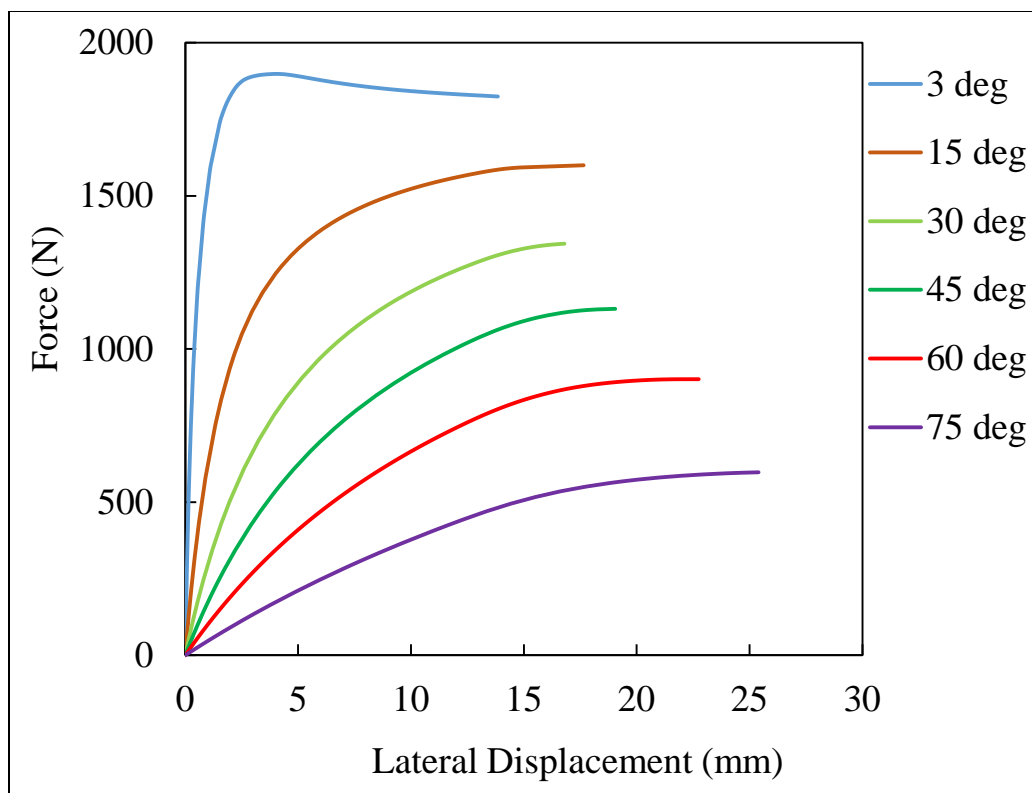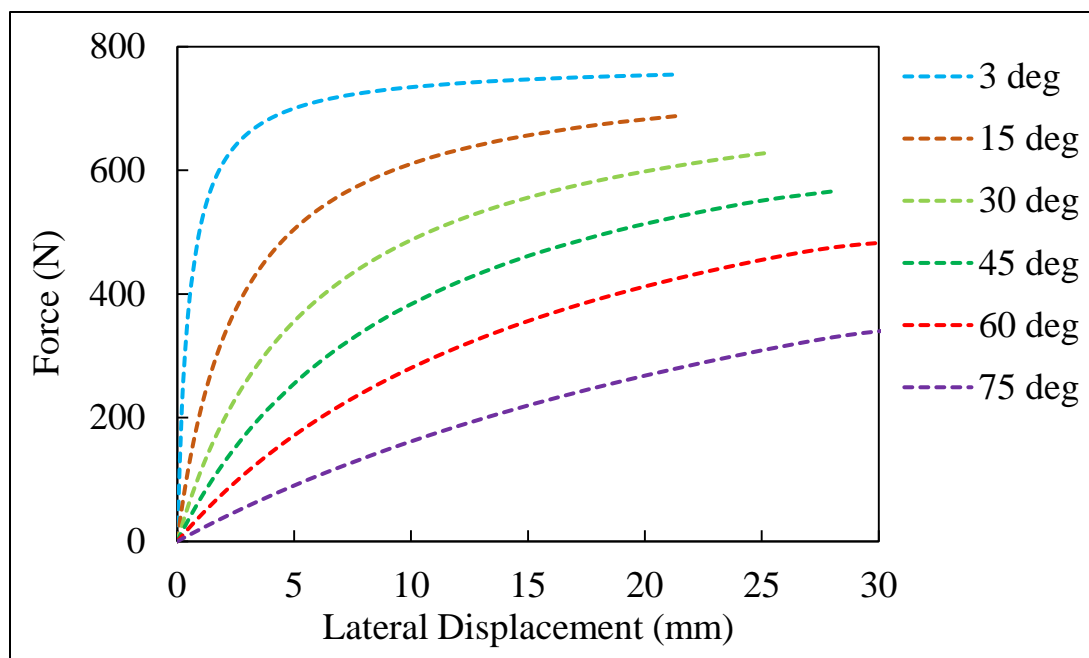Fig. 2.11: Force-displacement plots of 532 mm fuel rod for clad only with inclinations

Fig. 2.12: Force-displacement plots of 532 mm fuel rod for Case 1 and clad only

Fig. 2.13: Force-displacement plots of 532 mm fuel rod for Case 2 and clad only

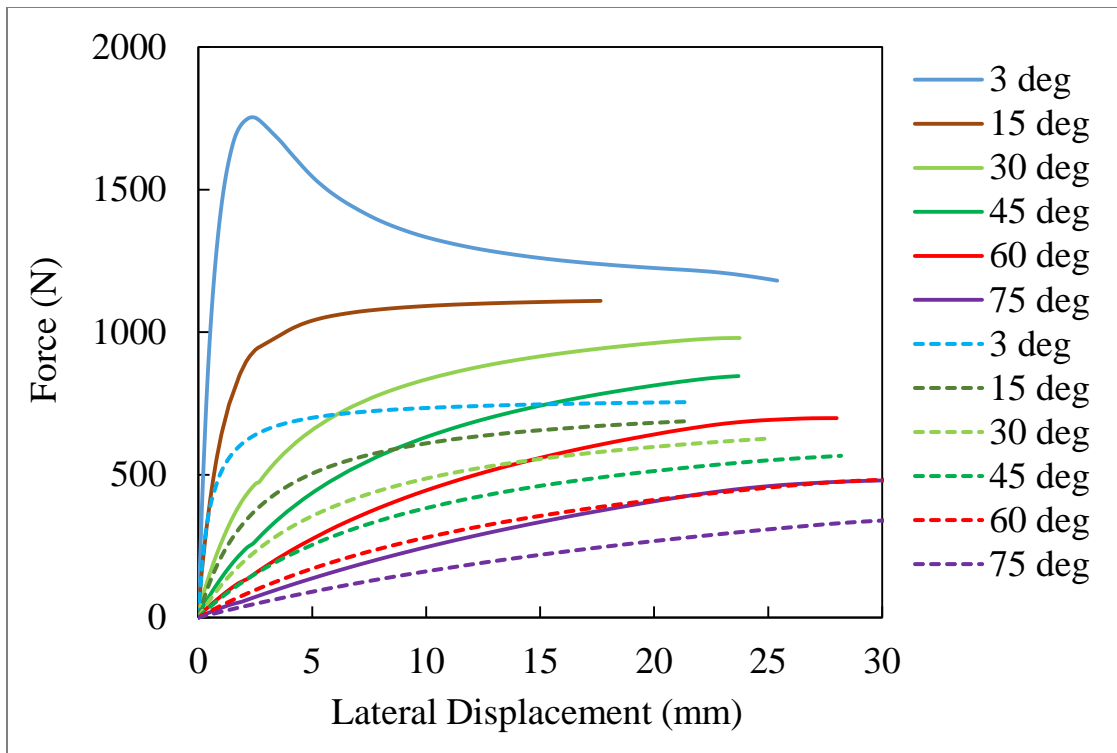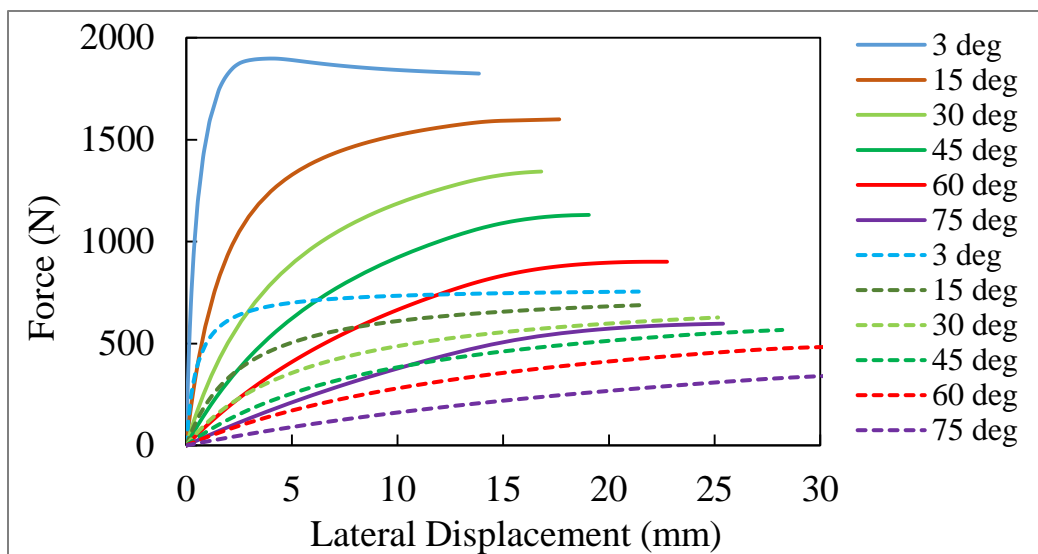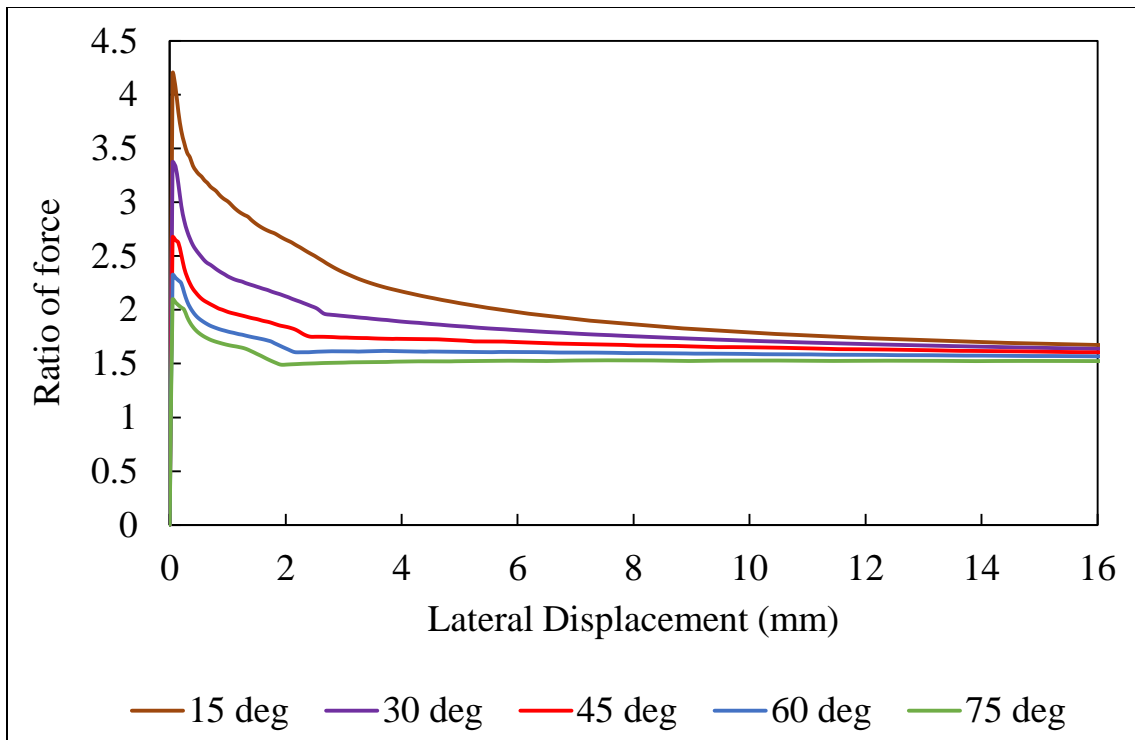Fig. 2.14: Normalized force-displacement plots for Case 1 with respect to clad only
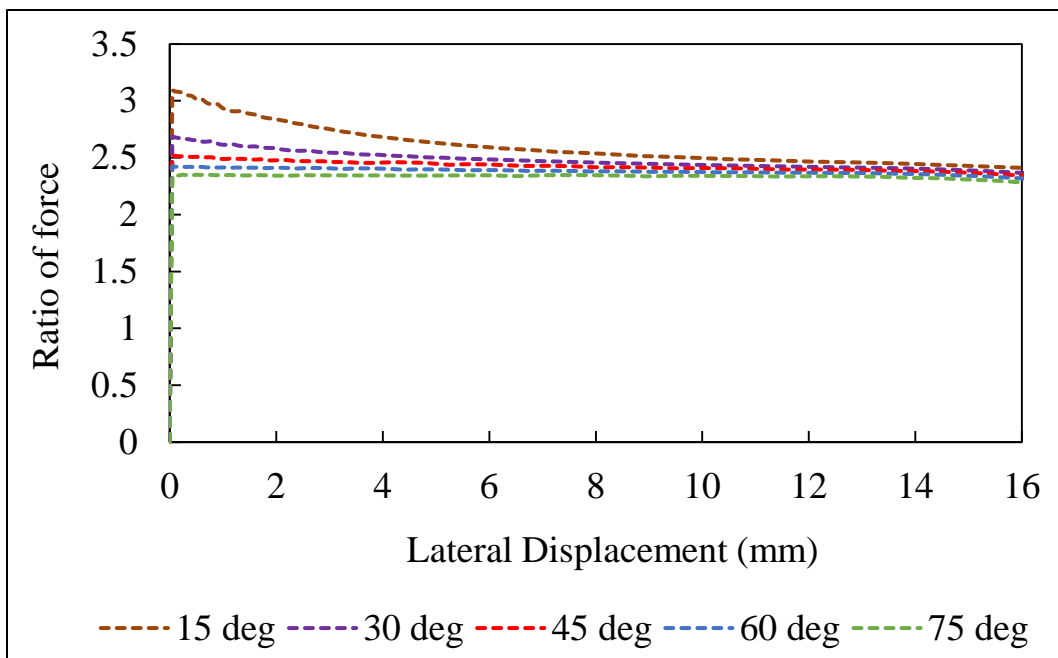

Fig. 2.15: Normalized force-displacement plots for Case 2 with respect to clad only
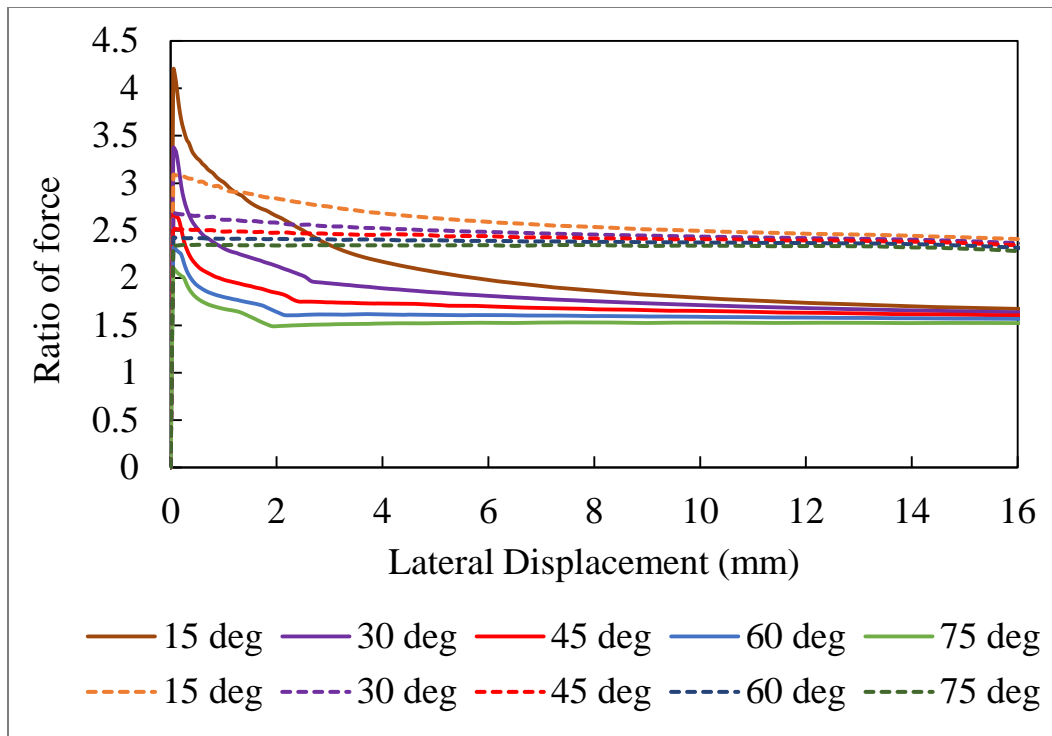
Fig. 2.16: Normalized force-displacement plots for Case 1 (solid), and 2 (dotted lines)

CHAPTER 3

QUASI-STATIC BUCKLING – EFFECT OF MATERIAL DEGRADATION

3.1 Material Degradation Mechanisms Related to Hydrogen in Fuel Cladding

Material degradation mechanisms can occur in SNF rods during long-term storage of dry storage casks (DSCs). Hydride-related degradation mechanisms include delayed hydrogen cracking (DHC), hydride reorientation, and hydride embrittlement. Among the hydride-related degradation mechanisms, the effect of hydride embrittlement is more pronounced for SNF rods after long-term storage.

The stress-strain curve of Zircaloy cladding is influenced by irradiation level, temperature, and the amount and orientation of hydrides within the cladding. The distribution of hydrides along the thickness of the cladding is nonuniform. Therefore, the stress-strain curve of cladding is defined by treating it as a three-layer composite material made up of Zircaloy matrix with embedded circumferential and radial hydrides. Fig. 3.1 shows the radial distribution of the hydrides in the fuel cladding (Machiels 2004). The hydrides concentration is thicker at the outer diameter of the clad compared to the inner diameter. The hydrides concentration is negligible at the inner diameter.

3.2 Fuel Rod Buckling Load Evaluation Including Material Degradation

This section evaluates the effect of material degradation on fuel rod buckling capacity. However, the buckling capacity of the typical 532 mm fuel rod will not decrease due to material deterioration because it is controlled by elastic buckling.

Fig. 3.2 shows the stress-strain curve used for the numerical simulation, as adapted from the experimental data from Machiels (2004) to have the same peak strength in the engineering curve. The engineering stress-strain curve of the irradiated clad is used to find the true stress-plastic strain curve, according to Equations 2, 3, and 4. This curve is then used for the numerical simulation in Abaqus.

The use of material deterioration parameters on the 532 mm fuel rod segment is not relevant on the buckling capacity because the component still is subjected to elastic buckling. Therefore, the slenderness ratio (KL/r) of the segment was reduced, by shortening the segment's length to record the material yielding and degradation effect.

Based on Euler equation, inelastic buckling only controls for lengths of 175.26 mm (6.9 in.) under simple supported conditions. Fig. 3.3 shows the Euler's curve for intact fuel rod cladding without any eccentricity.

From the calculations and the Euler's curve, the length of the fuel rod has to be less than 175.26 mm in the simply supported condition (K = 1) for the inelastic buckling to control. This simply supported length (i.e., the length of the fuel rod between the spacers) is larger than 175.26 mm in all fuel assemblies. However, the equivalent KL/r threshold can take place at the end cantilever segment. Therefore, the buckling analysis for the end cantilever segment is required to see the effect of degradation.

3.3 Length of the End Cantilever Segment of the Fuel Rod

Based on dimensions of the spacers (Adkins et al., 2013) for fuel assembly, the distance from the base of rod's bottom nozzle to the bottom first spacer grid is 87.681 mm (3.45 in.). Assuming a cantilever condition (i.e., K = 2), the Euler equation and the plastic limit indicate that inelastic buckling will control the rod's capacity if the cantilever's length is less than 88.9 mm (3.5 in.). Then, buckling behavior of the end cantilever segment would be controlled by inelastic buckling.

3.4 Analysis of 140 mm (5.5 in.) Simply Supported Fuel Rod

To assess the effect of yielding and material degradation on the buckling capacity, a simply supported fuel rod segment of length 140 mm is modeled. The results would be equivalent to those of a cantilever of 70 mm. The results for the linear Eigen value analysis and nonlinear Riks analysis, with and without degradation, are presented in the Figs. 3.4 and 3.5, respectively.

The buckling capacity for the 140 mm Case 1, with a 0.1 mm imperfection is 28,680 N, while with the capacity for the clad with linear material properties is 29,630 N. After the inclusion of degradation mechanism of the clad by using degraded true stress-plastic strain data, the buckling capacity decreased to 27,830 N. Therefore, the effect of degradation of clad is seen on the buckling capacity for 140 mm length of fuel rod for the simply supported condition. Thus, material deterioration that results in a more brittle plastic stress-strain curve affects the buckling capacity of end cantilever segments. However, these end segment are not expected to fail because its buckling capacity is one order of magnitude higher than that of the typical 532 mm segment.
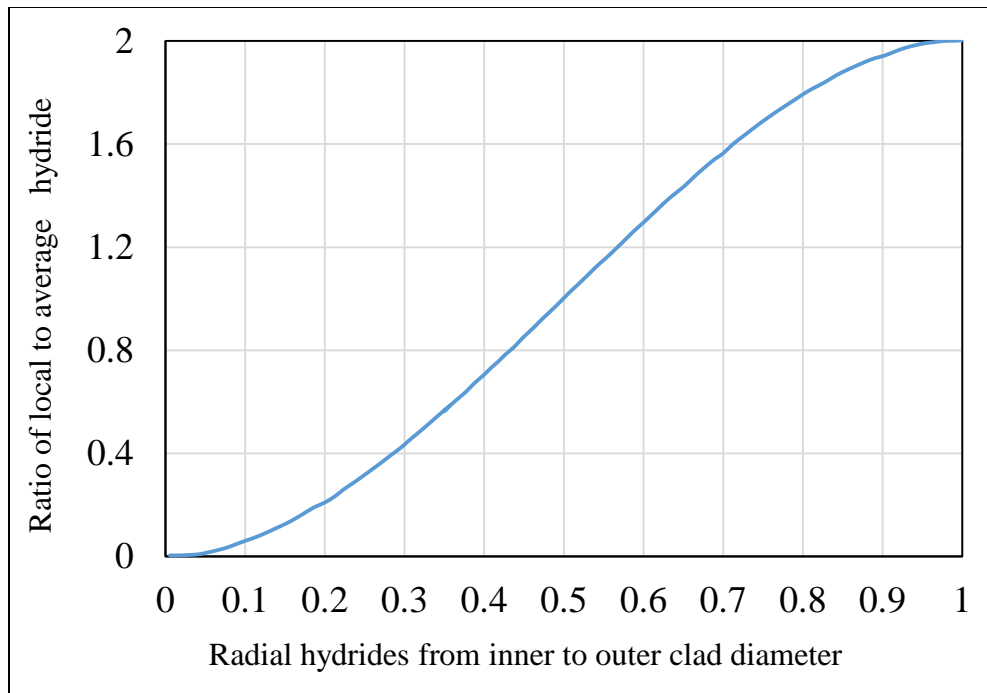
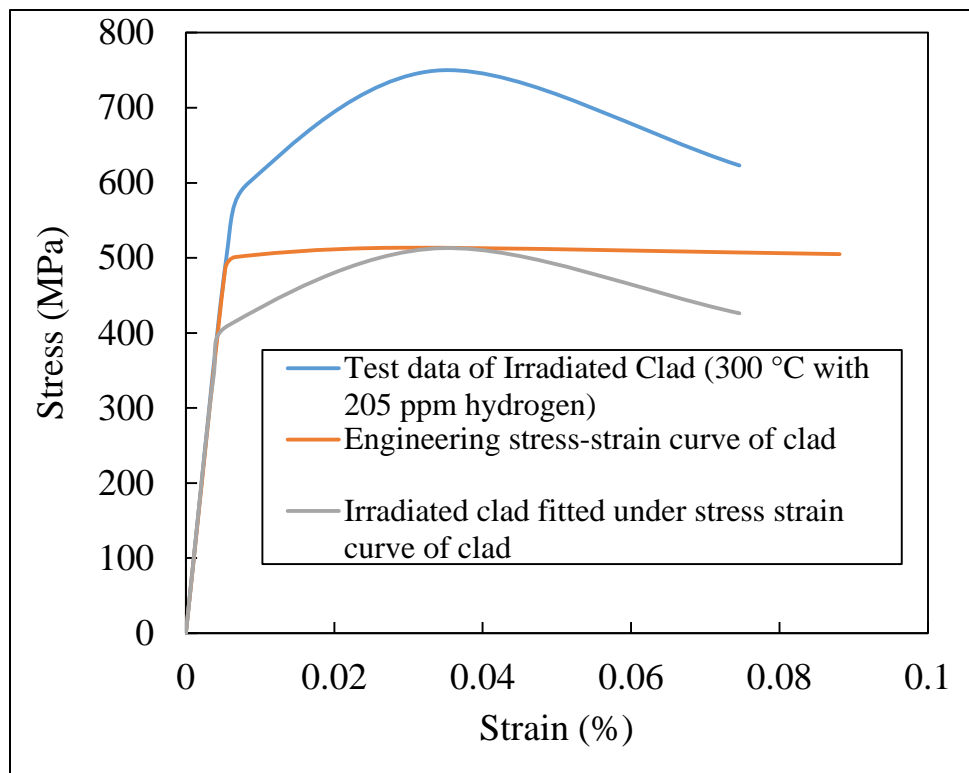Fig. 3.1: Distribution of hydride in cladding (modified after Machiels 2004)

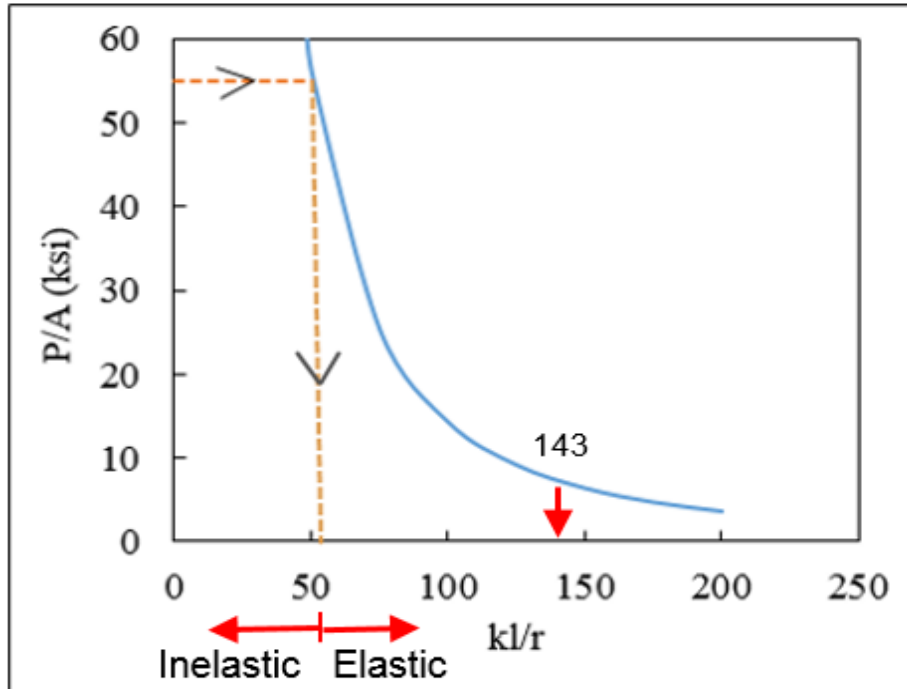Fig. 3.2: Cladding stress-strain relationship

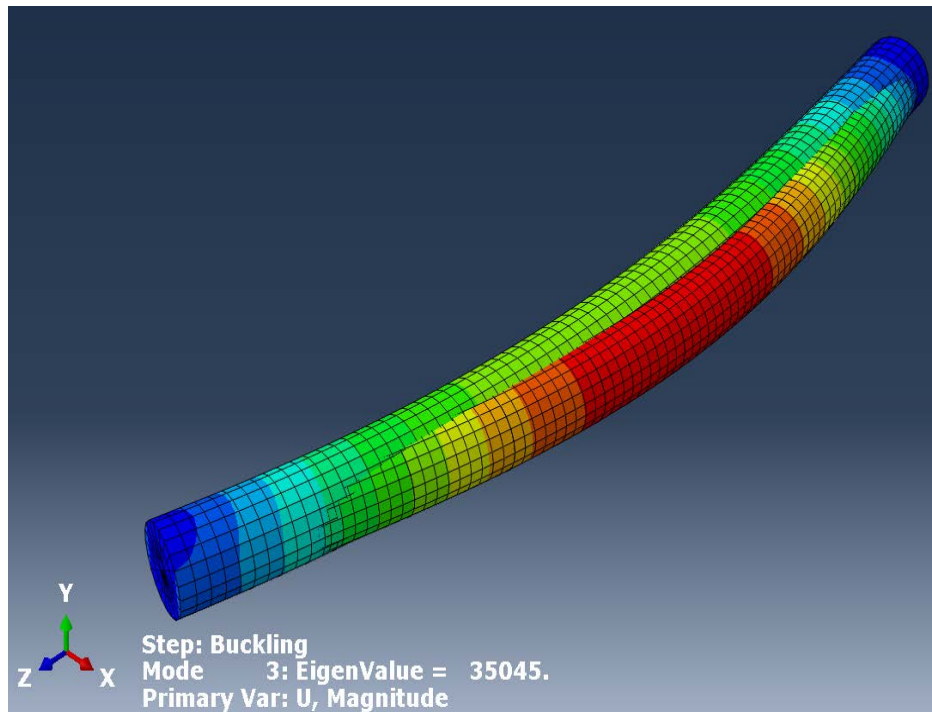Fig. 3.3: Euler's curve for fuel rod cladding

Fig. 3.4: Eigen value for Case 1 of 140 mm fuel rod for the vertical case
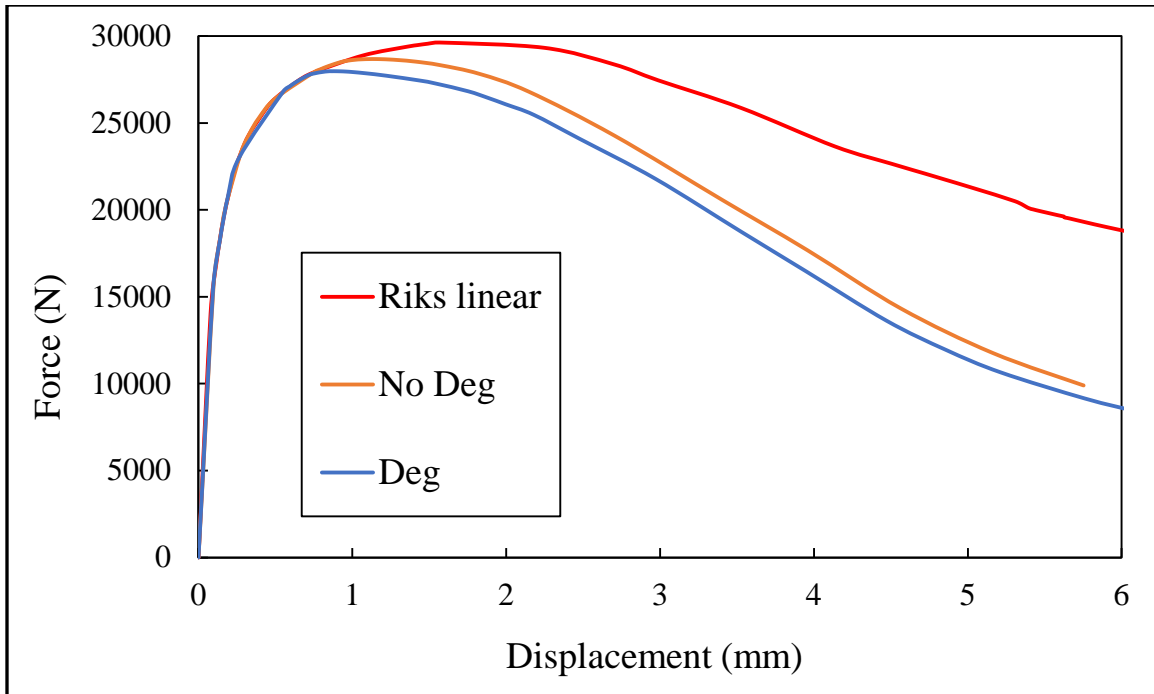
Fig. 3.5: Load-displacement plots of Case 1 for 140 mm fuel rod

CHAPTER 4

DYNAMIC IMPACT ANALYSIS

4.1 FE Model Description and Inputs

The dynamic impact analysis studies the accidental drop of cask during transportation. The structural integrity of a cask can be compromised because of an accidental drop during transportation. Fuel rods may buckle between spacer grids due to impact loads.

The major components of the cask model include the transportation cask, fuel basket, fuel rod, and impact limiters. The numerical analysis represents a 9 m. vertical drop of a fuel rod inside a cask against a rigid surface. The kinetic energy during impact is significantly absorbed by the impact limiters, but the transportation cask and internals still are subjected to large decelerations. The analysis evaluates the behavior of a fuel rod with three 532 mm segments (total 1596 mm) located in a cask with impact limiters.

4.1.1 Material Properties and Dimensions

The maximum lateral displacement of the center fuel rod in a fuel assembly is limited by rod-to-rod contact (Fig. 4.1). Based on the maximum possible lateral deflection of a fuel rod located in the center of the fuel assembly, a box with lateral clearance of 30 mm from the fuel rod is used. The total dimension of the box is 71.54×71.54 mm.

The fuel rod is connected to the box by four nonlinear springs acting in two orthogonal directions at every 532 mm (Fig. 4.2). These nonlinear springs represent the spacer grid in the fuel assembly. The spring characteristics in Fig. 4.3 are based on the spring model from Sanders et al. (1992). The springs are assumed to be fully relaxed (i.e., there is no preload), and are attached to the inner section of the box.

Impact limiters are provided at the ends of the cask to dissipate the kinetic energy of the cask during drop impact. Rajendran et al. (2005) used polyurethane foam as impact limiters in impact drop experiments on a 380 kg cask model for heights varying from 0.52 to 7.5 m., reducing the cask peak acceleration approximately 16 times. These polyurethane foam impact limiters (Matweb, 2015) are used in the analysis to limit deceleration forces.

Neutron shield plates are added inside the cask at top and bottom to limit the impact force in the inner box. According to Zencker et al. (2013), insertion of neutron shielding plates at the bottom prevents the upward bending of the cask bottom. Zencker et al. performed cask drop simulation to study reliability of cask designs under mechanical loads. Neutron shield properties and dimensions are taken from Adkins et al. (2013). The insertion of the neutron shield in the model reduces the highly stressed areas at the bottom of the cask.

There is a 10 mm clearance from the fuel rod to the steel box at top and bottom. Also, a 2 mm gap exists between the top of the pellet and the clad, which is connected by a linear plenum spring (Fig. 4.4) with stiffness k = 4 N/mm (Lee et al., 2010). According to Lee et al. (2010), a precompression force must be applied in the spring, which is at least six times the weight of the pellets to keep them in place after impact. Therefore, a concentrated load of 150 N, equivalent to six times the pellets weight in a 3,658 mm rod,

is applied at the top of the end pellet.

Table 4.1 presents the material model parameters and dimensions used in the cask assembly model taken from Adkins et al. (2013). The longitudinal section of the cask assembly is shown in Fig. 4.5.

4.1.2 Kinematic Constraints

The fuel rod is connected to the box by nonlinear springs in four directions at every 532 mm. These nonlinear springs represent the spacer grid in the fuel assembly, which allows limited lateral displacement between rod and spacer boundary.

General contact interaction is used for surfaces that may be in contact with each other, but not bonded. The friction coefficient for these contact surfaces is assumed as 0.25 (Williamson and Knoll, 2009). General contact accurately represents uniform contact tractions irrespective of mesh details (Harkness, 2009). In this explicit dynamic analysis, the general contact interaction approach provided more stable results than surface-to-surface contact, irrespective of mesh size and stress variation.

A tie constraint is used to simulate a bonded condition between impact limiters and the cask, and between cask and the neutron shield. Solid reduced integration linear brick elements (e.g., C3D8R) mesh elements are used for the cask and impact limiters.

4.1.3 Loading

A lumped mass of 1.4 kg is added at the top end of the pellet. This is the mass corresponding to the remaining length of a typical fuel rod, in addition to the 1,596 mm length segment used in the model. Gravity load is included in the model to incorporate the

self weight of the cask model. To reduce the analysis time, an initial velocity of 13,140 mm/s is included in the model (Fig. 4.6) in the Z direction. This is the velocity of the cask after a free fall from a height of 8,800 mm. Then, the cask assembly is dropped 200 mm onto an unyielding surface, which is simulated in Abaqus with a rigid surface.

4.2 Dynamic Impact Analysis Results

4.2.1 Vertical End Drop

The primary objective of this study is to evaluate the structural integrity and performance of SNF rods, following a drop impact from a height of 9 m. Large cask deformations compress the fuel rod, and may lead to fuel rod buckling failure. Therefore, impact limiters are incorporated to absorb part of the kinetic energy and reduce cask decelerations.

Fig. 4.7 shows the Von Mises (VM) stresses in the cask assembly after impact. The deformations and large stresses are highly localized at the bottom of the cask. However, the maximum stresses of about 47 MPa are within the material elastic regime, given that the yield stress is 207 MPa for 304 stainless steel.

Figs. 4.8 and 4.9 show the velocity and acceleration time histories, respectively, measured at the bottom center of the cask, which is expected to experience the highest impact effects. The acceleration time history (ATH) is obtained by differentiating velocity time history (VTH), because the ATH directly obtained in Abauqs exhibited large variations before the impact and greater acceleration after impact, possibly because of the noise in the high frequency acceleration wave. The VTH in Fig. 4.8 shows the linear increase of velocity from 13,140 mm/s (corresponding to a fall height of 8,800 mm) to

13,290 mm/s (fall height of 9,000 mm), and then the velocity drops after the impact takes place at 0.02 s.

The ATH of the cask bottom (Fig. 4.9) has a peak of about 42 g. after impact. This is the demand from the 9 m. drop impact onto a rigid surface. The demand is less than a quarter of the 200 g. safety margin recommended by NUREG (2014) to prevent clad breaching. Nevertheless, the fuel rod will experience higher decelerations than the cask because of dynamic interaction between the fuel rod and steel box due to the 10 mm gap. The deceleration at the fuel rod level is expected to be higher compared to that at the cask level. The peak deceleration at the clad bottom is 126 g. (Fig. 4.10).

Buckling is not readily observed in the fuel rod following the 9 m. vertical drop because no initial rod imperfections or perturbations are included in the model, unlike the imperfection of 0.1 mm in the quasi-static model. Fig. 4.11 shows lateral displacement time history (DTH) at the center of bottom fuel rod segment, with a maximum displacement of 0.7 mm. The displacement from the quasi-static analysis for the peak buckling load is 1.6 mm for the vertical end drop of Case 1. Case 1 has the pellet-cladding radial gap of 80 μm and pellet-pellet in contact, but not bonded. Therefore, the fuel rod has not failed in buckling after the vertical drop impact from the dynamic impact analysis.

4.2.2 Impact at Different Inclination Angles

The inclination of the cask is varied to represent other potential impact loading conditions. Fig. 4.12 shows the 15° cask inclination with respect to the vertical during impact. The inclination results in asymmetric boundary conditions that lead to fuel rod buckling. The lateral DTH at the center of bottom fuel rod segment in Fig. 4.13 shows the

maximum displacement of 3 mm for 3° cask inclination and 8 mm for 15°. The displacement from the quasi-static analysis for the peak buckling load is 2.5 mm for the 3° and 5 mm for the 15° drop of Case 1. Therefore, the end fuel rod segment is likely to exhibit buckling failure following the 3° and 15° drop angle impact. Fig. 4.14 shows the ATH of the clad following the 3° and 15° drop angle. The acceleration at the clad bottom is 134 g. for the 3° drop and 148 g. for the 15° drop.

Table 4.1: Material model parameters and dimensions (Adkins et al., 2013)

| Part	Material	Density (kg/m^3)	E (GPa)	Poisson ratio	Dimensions (mm) Diameter (Ø),Length (L) Breadth (B),Thickness (t)
Impact limiter	Polyurethane foam	80	2.0	0.30	Ø = 3250, t = 900
Cask	304 Stainless steel (SS)	7,860	192.0	0.29	Ø = 2184, L = 2488
Neutron shield	Neutron shield	1,680	4.0	0.30	Ø = 1784, t = 132
Basket box	304 SS	7,860	174.0	0.45	B = 71.54, L = 1624
Clad	Zr-4	6,590	99.3	0.37	Ø = 10.54, L = 1600
Pellet	Uranium dioxide (UO$_2$)	10,290	166.0	0.21	Ø = 9.18, L = 14
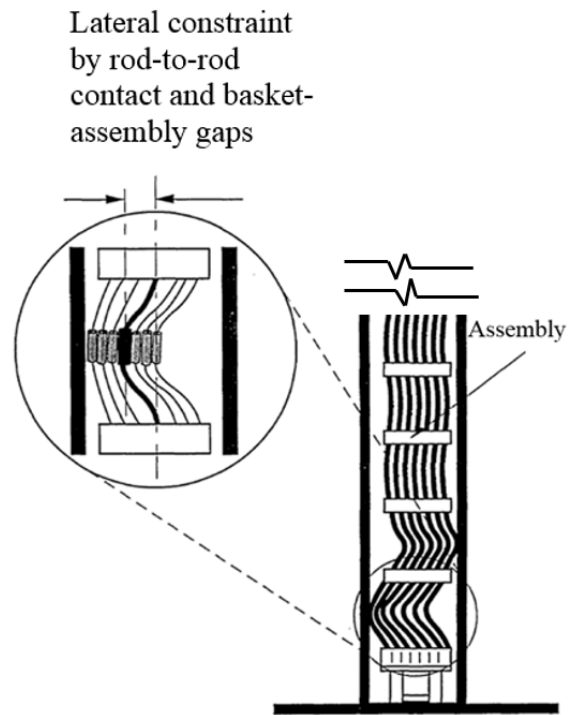
Fig. 4.1: Lateral constraint by rod-to-rod contact (modified after Sanders et al., 1992)
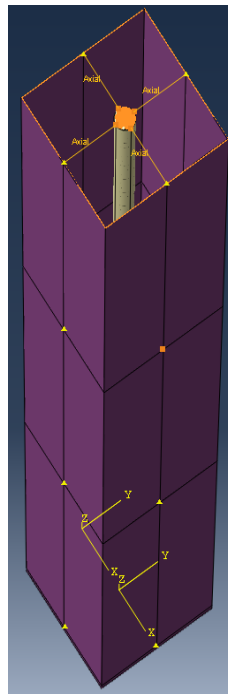

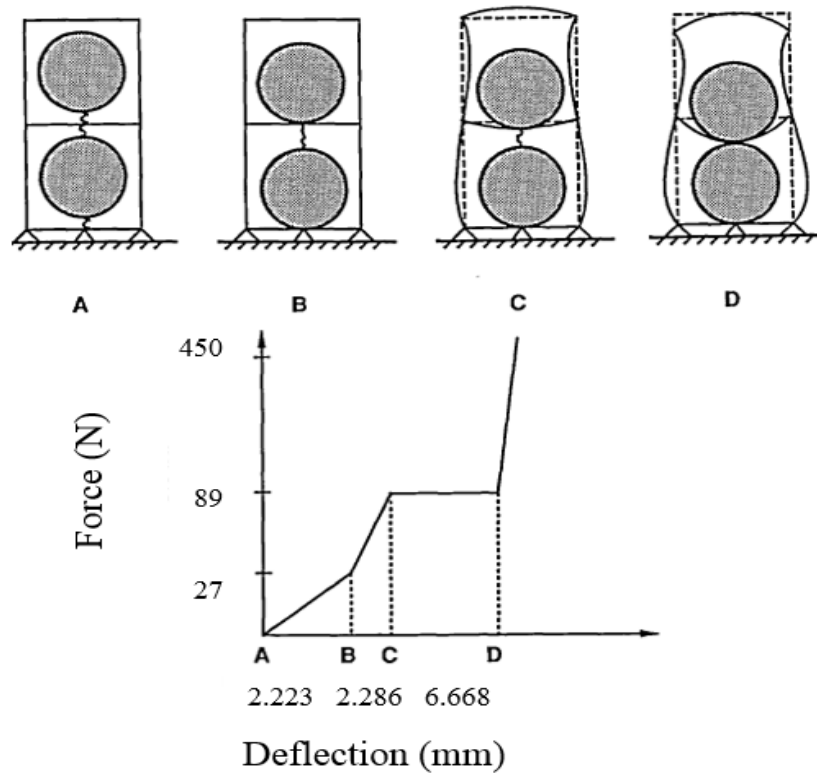Fig. 4.2: Connection of nonlinear springs to the box

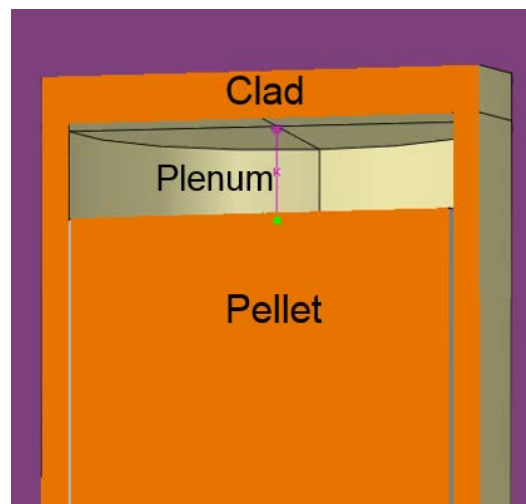Fig. 4.3: Spacer grid response (modified after Sanders et al., 1992)

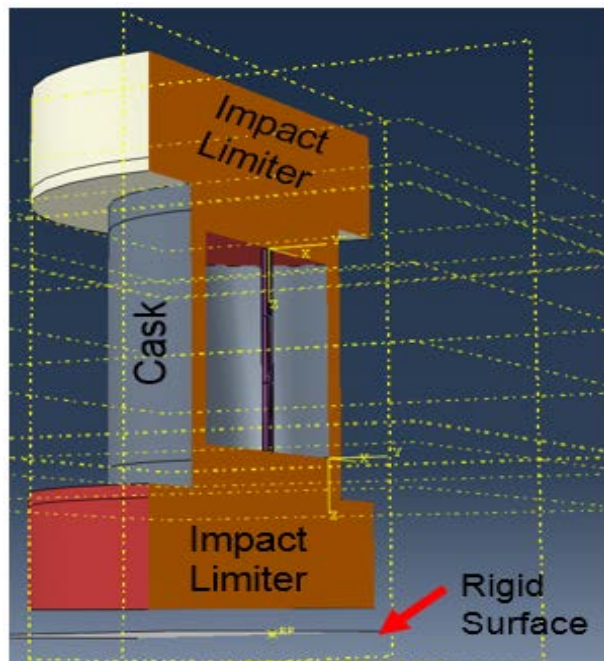Fig. 4.4: Linear plenum spring between end pellet and clad

Fig. 4.5: Longitudinal section of the cask assembly

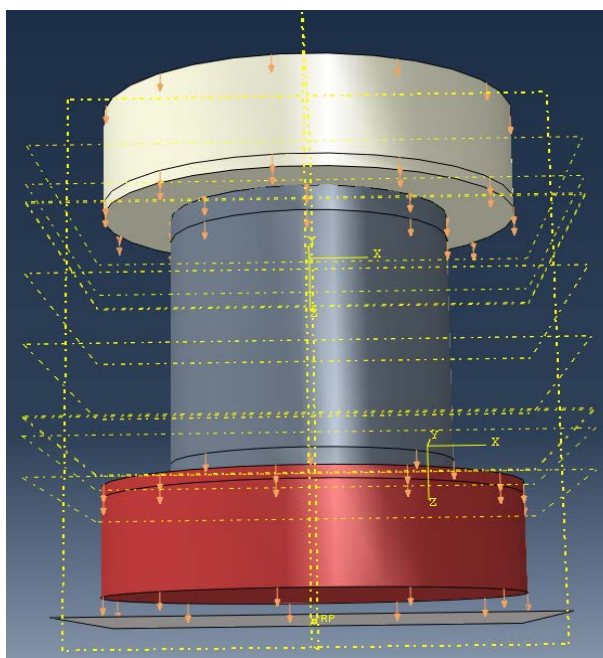Fig. 4.6: Loading in the cask assembly
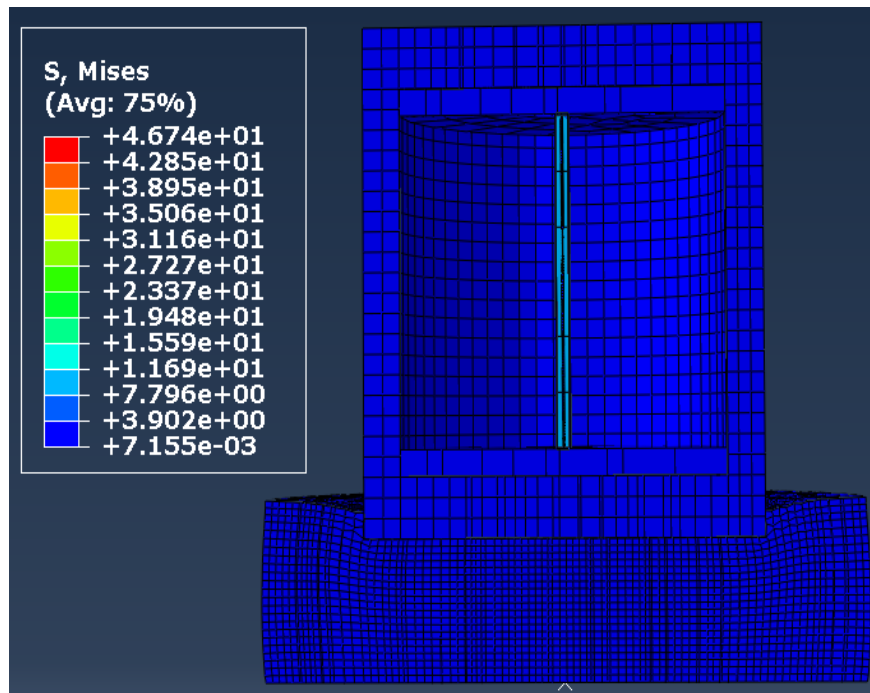
Fig. 4.7: VM stresses (MPa) in the cask assembly after end on impact

Fig. 4.8: Velocity time history at the cask bottom center

Fig. 4.9: Acceleration time history at the cask bottom center

Fig. 4.10: ATH at the clad bottom

Fig. 4.11: Lateral DTH at the center of bottom fuel rod segment for vertical drop

Fig. 4.12: Cask model inclined 15° to the vertical

Fig. 4.13: Lateral DTH at the center of bottom fuel rod segment
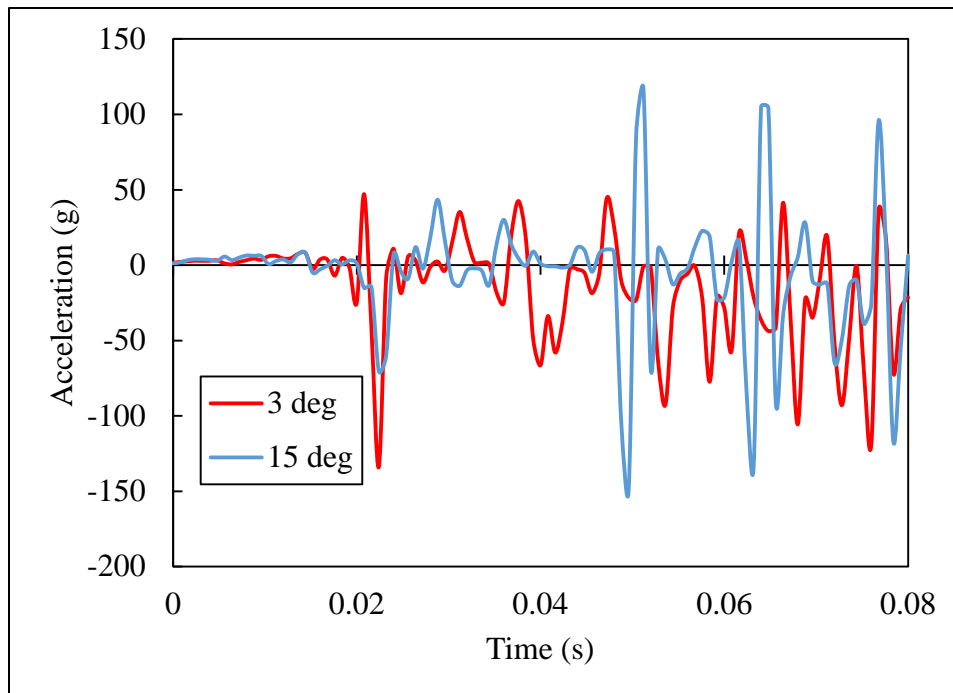
Fig. 4.14: ATH of the clad bottom

CHAPTER 5

SUMMARY AND CONCLUSIONS

5.1 Summary

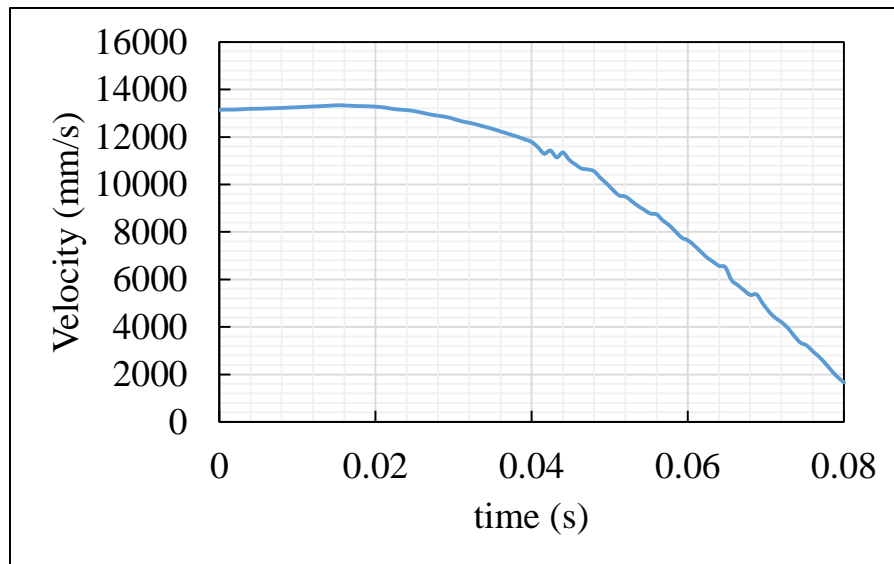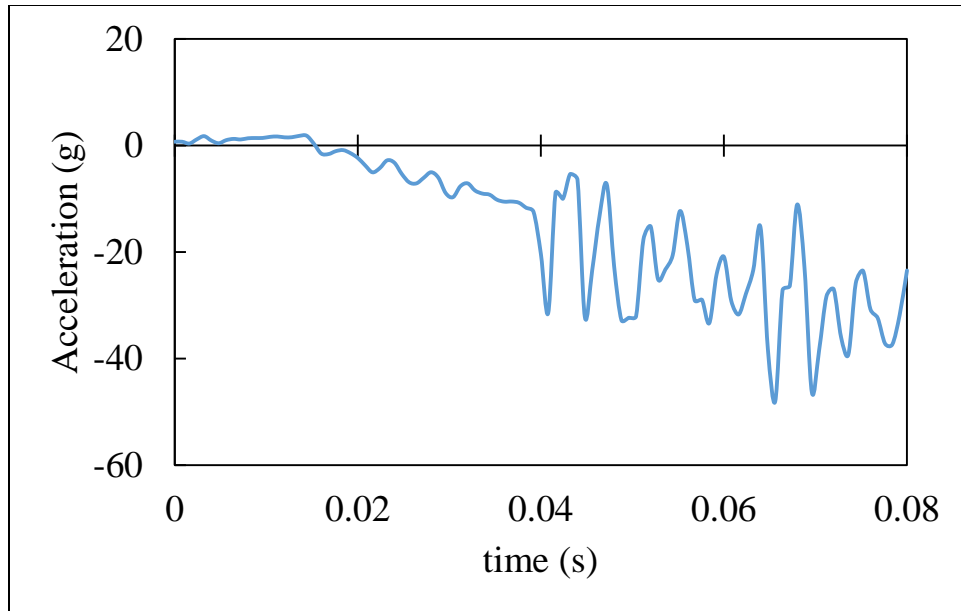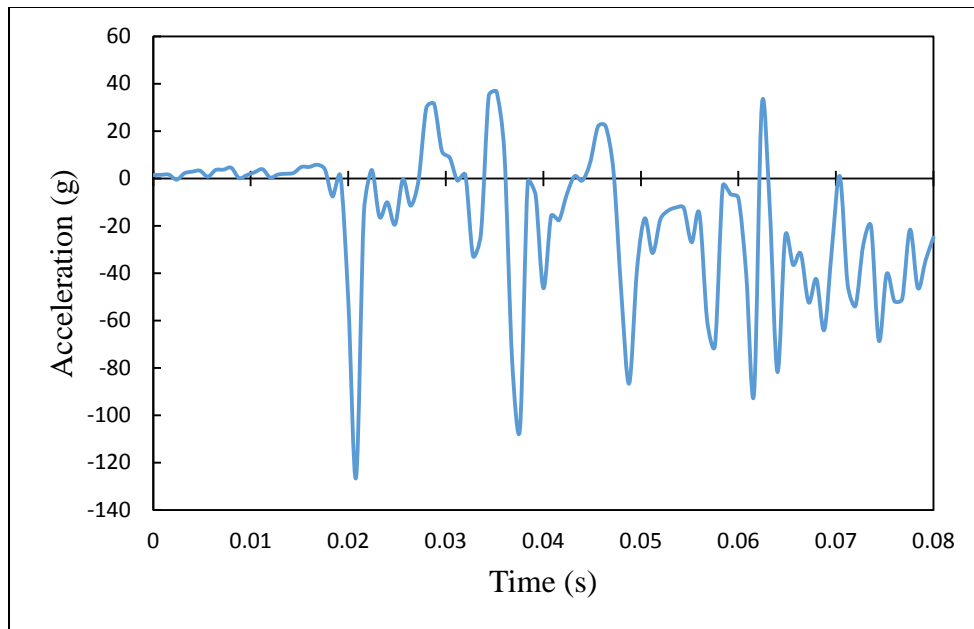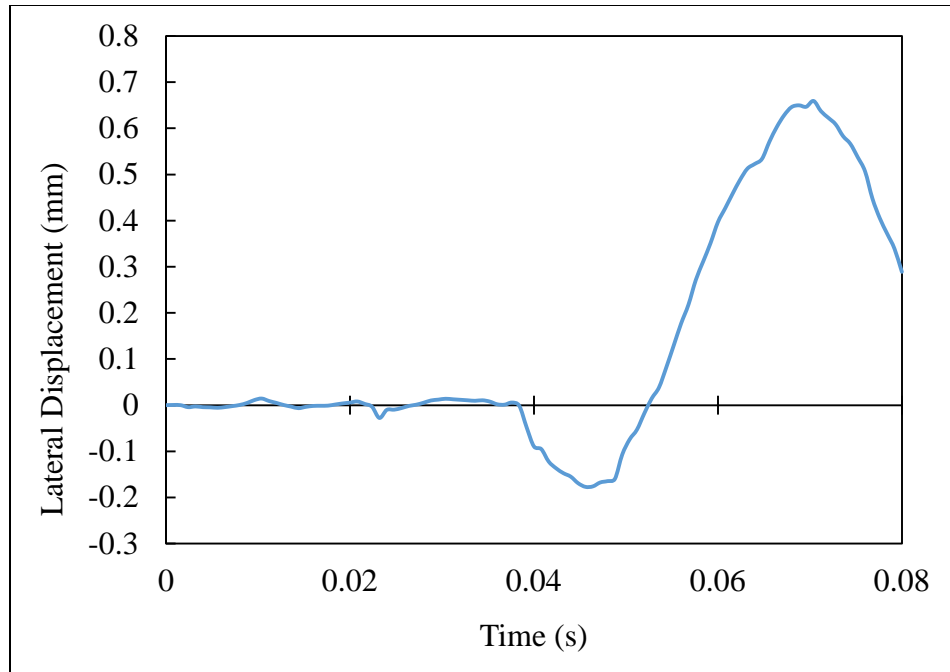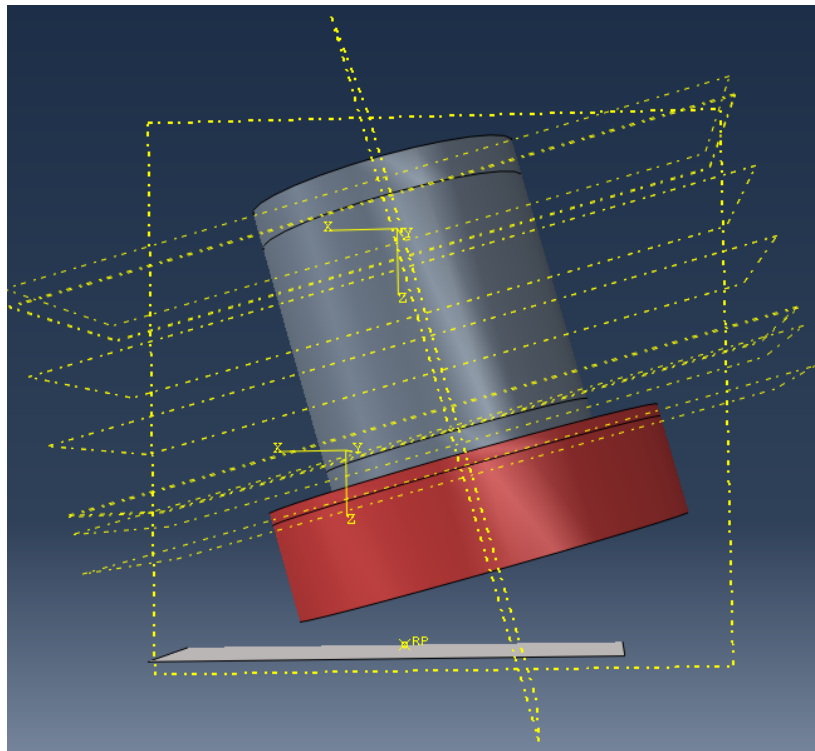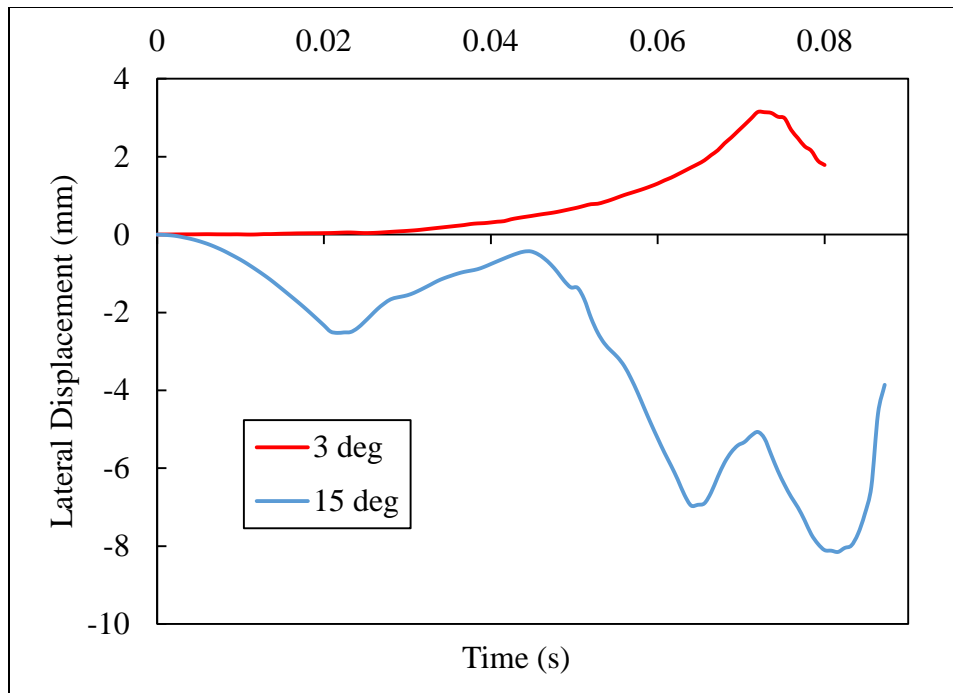This study evaluates the structural integrity of spent nuclear fuel (SNF) rods due to potential impact loads during transportation. For this purpose, linear and nonlinear buckling analyses of typical fuel rod segments are performed in the finite element (FE) software Abaqus, under static and dynamic loading conditions. The study also assesses pellet-cladding interaction (PCI) effects and degradation mechanisms on the buckling behavior of SNF rods during transportation.

To investigate the effect of PCI, numerical simulations are performed in the 532 mm fuel rod segment for three different cases: (1) pellet-cladding radial gap of 80 μm and pellet-pellet in contact; (2) PCI and pellet-pellet in contact; and (3) PCI and pellet-pellet bonded. For the study of degradation mechanisms, the effect of hydride embrittlement of the irradiated clad after long-term storage is incorporated into the analyses. The findings are summarized below.

The presence of pellets in Case 1, even without PCI effects, increases the buckling capacity almost three times with respect to that of the clad only rod segment, from 771 N in clad only to 2,173 N. However, after the bifurcation point, the strength of the Case 1 rod rapidly decreases and approaches the buckling capacity of the clad only segment.

Therefore, the additional Case 1 buckling capacity provided by the pellets is unstable, and it can only be considered for lateral displacement limited to 2 - 3 mm.

The fuel rod buckling capacity increases 20% for Case 2 when PCI is taken into account, from 2,173 N in Case 1 to 2,624 N in Case 2. The most important effect, however, of the pellet-cladding bonding is that the strength for Case 2 is only reduced 20% after the bifurcation point.

The capacity of Case 3 only increases 5% compared to that of Case 2, indicating that the influence of pellet-pellet bonding on buckling capacity is less relevant than PCI. The pellet-clad and pellet-pellet bonding results in a solid composite fuel rod. The main effect of pellet-pellet bonding is on the rod's stable postbuckling behavior.

The stresses of the 532 mm-long fuel rod segment for Cases 1, 2, and 3 are 69, 76, and 80 MPa, respectively. The stresses are about 20% of the yield strength of 381 MPa. This result proves that the buckling behavior of the 532 mm fuel rod is controlled by elastic buckling because of its large slenderness ratio (KL/r =143). It can also be corroborated by the fact that the load-displacement plot with the linear and nonlinear material properties overlapped. Therefore, the 532 mm fuel rod would fail because of elastic instability before yield strength is achieved.

The fuel rod buckling capacity decreases as the inclination angle at impact increases. The results show that the beneficial effects of fuel pellets in terms of buckling capacity are significantly reduced as the rod inclination increases. For example, even for a small inclination angle of 15° with respect to the vertical, there is a 50% reduction for Case 1 and 40% for Case 2, relative to the vertical impact scenario.

The buckling capacities of Cases 1 and 2 are normalized with respect to the capacity

of the clad only. For small displacement, the Case 1-to-clad only ratios exhibit large ratios that rapidly decrease and stabilize at about 1.5 for all the orientation angles. Note that the stabilization at a ratio of about 1.5 for Case 1, for horizontal (or quasi-horizontal) impact conditions, is mainly caused by the pellets being in perfect contact in the FEM. The large initial values indicate that pellets greatly stiffen the fuel rod when the orientation is almost vertical. However, as the orientation angle at impact increases, the pellet contribution decreases. For Case 2-to-clad only ratios, the ratios approach a value of about 2.5 for large displacements, indicating that PCI composite action is partially retained even if the orientation angle is relatively large. For Case 2, the FEM does not lead to an overestimation for close to horizontal impact loading scenarios because the pellets cannot move longitudinally due to PCI.

Based on Euler's buckling equation, inelastic buckling controls fuel rods of lengths 175.3 mm (6.9 in.) or less, under simple supported conditions, or a length of 87.7 mm (3.45 in.) when assuming a cantilever condition. Based on these conditions, only the end cantilever segments may exhibit nonlinear buckling behavior. Therefore, the cladding degradation effect can only be observed on the buckling capacity of the 140 mm (5.5 in.) length of fuel rod for a simply supported condition. Consequently, material deterioration may only affect the end cantilever segments. This cantilever segment, however, is not expected to fail because its buckling capacity of 27,830 N is one order of magnitude higher than that of the 532 mm segment of 2,173 N.

In the dynamic impact analysis for a drop height of 9 m, the maximum Von Misses (VM) stresses in the cask are about 47 MPa, which are below the yield strength of 207 MPa for 304 stainless steel. Thus, the cask material behavior is still within the elastic range.

The acceleration time history of the cask bottom shows the maximum peak around 50 g. after impact, below the safety margin of 200 g. (NUREG, 2014) to prevent clad breaching. Therefore, for the provided material properties and dimensions, the fuel rod clad will not fail due to elastic or inelastic buckling following the 9 m. drop in the cask assembly.

The lateral DTH at the center of bottom fuel rod segment shows a maximum displacement of 0.7 mm for the vertical end drop, which is less than the displacement of 1.6 mm from the quasi-static analysis for the peak buckling load.

For the inclined drop impact, the transverse DTH at the center of bottom fuel rod segment results in a maximum displacement of 3 mm for a 3° cask inclination, and 8 mm for a 15° inclination. The displacement from the quasi-static analysis for the peak buckling load is 2.5 mm for the 3° and 5 mm for the 15° drop of Case 1. Therefore, the end fuel rod segment is close to buckling failure for the 3° and 15° drop angle impact scenarios. The fuel rod is within elastic limit, because of which it may recover after the maximum lateral displacement.

5.2 Overall Conclusions

The buckling capacity of a fuel rod depends on the bonding conditions between the clad and pellets. During the early stage of fuel rod storage when there is no bonding between clad and pellets, the buckling capacity of a fuel rod can be taken as the capacity of the clad only. This is conservative because the capacity of a fuel rod eventually converges to the capacity of clad only for larger displacements. The Pellet-Cladding Interaction (PCI) has a significant effect on the fuel rod capacity. The capacity with the

PCI effect is three times the capacity of the clad only. The condition with the pellet-pellet bonding and PCI is highly unlikely and the capacity in such scenarios cannot be taken into consideration.

The effect of hydride embrittlement is only relevant for the end cantilever segments with lower slenderness ratio. However, the buckling capacity of cantilever segments is higher than that of the regular simply supported segments. Therefore, there would not be any effect on the overall buckling performance of a fuel rod because of the effect of degradation mechanisms related to hydride embrittlement.

5.3 Future Work

The recommendations for future research would be to perform laboratory experimental tests for pure compression test and dynamic drop test. The tests are useful for the validation of the numerical models.

REFERENCES

ABAQUS/Explicit Version 6.14. (2014). ABAQUS, Inc.

Adkins, H., Geelhood, K., Koeppel, B., Coleman, J., Bignell, J., Flores, G., Wang, J-A., Sanborn, S., Spears R., & Klymyshyn, N. (2013). Used nuclear fuel loading and structural performance under normal conditions of transport-modeling, simulation and experimental integration RD&D plan. *Used Fuel Disposition Campaign.* FCRD-UFD-2013-000135, U.S. DOE, Washington D.C.

Brown, J. (1997). Characterization of MSC/NASTRAN & MSC/ABAQUS elements for turbine engine blade frequency analysis. *MSC Aerospace Users Conference Proceedings.* Newport Beach, California.

Harkness, H., & Ang, G. (2009). General contact for implicit FEM. *Proceedings of NAFEMS World Congress.* Crete, Greece.

Machiels, A. (2004). Failure criteria for Zircaloy cladding using a damage-based metal/hydride mixture model. *EPRI,* Palo Alto, California, 1009693.

Matweb. (2015) http://www.matweb.com/ATI WahChangZirconiumAlloyZircaloy-4.

Rajendran, R., Sai, P., Joy, S., Krishnamurthy, K., & Basu, S. (2003). Vertical impact shock response of a cask model on a rigid unyielding surface. *International Journal of Impact Engineering, 31*(3), 307-325.

Ramasamy, U., Ibarra, L. F., & Medina, R. (2015). Buckling behavior of spent nuclear fuel rods. *Trans of SMiRT, 23.* Manchester, UK.

Ramsey, C., Monika, W., & Schwartz, M. (1987). Dynamic impact effects on spent fuel assemblies. *UCID21246.* Lawrence Livermore National Laboratory, Livermore, California.

Sanders, T., Seager, K., Rashid, Y., Barrett, P., Malinauskas, A., Einziger, R., Jordan, H., Duffey, T., Sutherland, S., & Reardon, P. (1992). A method for determining the spent fuel contribution to transport cask containment requirements. *SAND90-2406.* Sandia National Laboratories, Albuquerque, New Mexico.

U.S. DOE. (1987). Characteristics of spent fuel, high level waste, and other radioactive wastes which may require long term isolation. *Proceedings of the international topical meeting on nuclear and hazardous waste management*. Pasco, Washington.

Williamson, R., & Knoll, D. (2009). Enhancing the ABAQUS thermomechanics code to simulate steady and transient fuel rod behavior. *Proceedings of Top Fuel.* Paris, France.

Zhan, Y., & Li, M. (2013). A comparative study on numerical buckling analysis for a cantilever steel pipe column under combined loads. *International Journal of Engineering Research, 2*(3), 253-256.